BIOCHEMICAL CHARACTERIZATION OF LPL FUNCTION

Cassandra Kay Hayne

A dissertation submitted to the faculty at the University of North Carolina at Chapel Hill in partial fulfillment of the requirements for the degree of Doctor of Philosophy in the Biochemistry and Biophysics Department in the School of Medicine.

Chapel Hill
2017

Approved by:

Saskia Neher

Dorothy Erie

Sharon Campbell

Eric Brustad

Henrik Dohlman

ABSTRACT

Cassandra Kay Hayne: Biochemical Characterization of Lipoprotein Lipase
(Under the direction of Saskia B. Neher)

Elevated triglycerides levels are an independent risk factor for the development of cardiovascular and metabolic diseases. Approximately one third of the American population suffers from hypertriglyceridemia. Lipoprotein lipase (LPL) is the rate-limiting enzyme for the hydrolysis of triglycerides from triglyceride rich lipoproteins (TRLs), which circulate in the blood. LPL also promotes clearance of circulating triglycerides by catalyzing the uptake of TRL remnant particles into the liver. For both its role in catalysis and lesser recognized role in lipoprotein uptake, LPL is an attractive therapeutic target for reducing circulating triglyceride levels and the subsequent risk of cardiovascular disease.

Studies to understand LPL function have thus far been limited by protein yields, particularly for human LPL. This thesis focuses on work undertaken to better understand the elements that contribute to LPL's successful function. First, I focused on pinpointing the benefit of a known, gain-of-function mutation, LPL^{S447X}. LPL^{S447X} is used in LPL gene therapy, but until now, there had been no clear mechanistic explanation for its gain-of-function. I next describe a new method for measuring LPL interactions and dynamics, using total internal reflection fluorescence microscopy to monitor single molecules of LPL. Finally, I conclude with a discussion of the ways these developments are moving the field forward.

To my mom.
My personal superwoman.
Her strength, love for others, and love for science are endless.

ACKNOWLEDGEMENTS

This thesis would not have been possible without the support of a wonderful mentor, Sasky. Thank you for providing endless encouragement, understanding, advice, support, and for checking my sass when needed. Few graduate students have such a positive disposition during their final years of graduate school, and I owe a huge amount of that to you for always helping me find a way forward. I am thankful you took a chance on me.

Next, a huge "thank you" to all the teachers and professors who have supported and challenged me during my academic career. My deepest appreciation to the various professors who have opened their labs to me over the last eleven years: Dr. Sue O'Dorisio and Professors Duane Bartak, Jeffery Elbert, David McClenahan, Madeline Shea, Martin Caffrey, Dorothy Erie, and of course Saskia Neher.

To my committee members, who have challenged me and encouraged me to keep pushing, "Thank you!". More importantly, thank you for sharing in my successes and keeping me looking past the failures. Sharon, Saskia, and Dorothy you have been dynamite female scientist role models and I cannot thank you enough for your guidance and support, especially this past year.

I would like to thank past and present members of the Neher Lab. My deepest appreciation to all of you who have joined me on my graduate school journey. You

helped me learn patience, humility, and overcome the challenges of science. Thank you for being my official cupcake taste testers. You all made lab a fun place to be and made it feel like a home. Along the way, I had the great privilege of training some excellent undergraduates, and I would like to particularly thank Lin Cao for being my mini-wing woman in the lab these last three years. In addition to the Neher Lab, I found a second lab home in the Erie Lab and would like to thank everyone who adopted me as a lab "foster member." Jake Gauer, thank you for teaching me the ropes of the scope, your passion for teaching was not lost on me.

Next, I would like the thank the National Science Foundation for providing me with a Graduate Research Fellowship as well as Global Research Opportunity Worldwide (GROW) Awards in conjunction with the Science Foundation of Ireland. These awards were some of the highlights of my graduate school experience. Thank you to Martin Caffrey and members of his lab, Nicole Howe and Susan Fetics, for welcoming me at Trinity as part of my GROW Awards.

My experience in graduate school would not be what it is without the help and assistance of so many people across the University of North Carolina at Chapel Hill, including the Graduate School (including a Dissertation Completion Fellowship), the Office of Graduate Education (and everyone in the biological and biomedical sciences program office), and the Department of Biochemistry and Biophysics. Thank you to the past and present administrative staff of the Department of Biochemistry and Biophysics, you have all helped me overcome various obstacles during my time at UNC.

On a more personal note, I would like to thank my entire family. My parents have never wavered in their support of my personal or academic endeavors. They provided

TABLE OF CONTENTS

LIST OF TABLES

LIST OF FIGURES

LIST OF ABBREVIATIONS AND SYMBOLS

%	percent
°C	degrees Celsius
±	plus or minus
<	less than
>	greater than
≥	greater than or equal to
Å	angstrom
ABPP	activity based protein profiling
AFM	atomic force microscopy
ANGPTL	angiopoietin-like protein
APOC-I	apolipoprotein CI
APOC-II	apolipoprotein CII
APOC-III	apolipoprotein CIII
APOA-V	apolipoprotein AV
BME	β-mercaptoethanol
BSA	bovine serum albumin
C-terminal, C-term	carboxyl terminal
$CaCl_2$	calcium chloride
Cl	chloride
cm	centimeter
CVD	cardiovascular disease

DGGR	1,2-Di-O-lauryl-rac-glycero-3-(glutaric acid 6-methylresorufin ester)
DMEM	Dulbecco's Modified Eagle Medium
DMSO	dimethyl sulfoxide
E	energy transfer
E. coli	Escherichia coli
EDTA	Ethylenediaminetetraacetic acid
EL	endothelial lipase
ELISA	enzyme-linked immunosorbent assay
emCDD	electron multiplying charge-coupled device
Ex	excitation
FBS	fetal bovine serum
FFA	free fatty acids
FRET	fluorescence resonance energy transfer
Fu	fluorescence unit(s)
g	g-force, gravitational acceleration
GAPDH	glyceraldehyde-3-phosphate dehydrogenase
GPIHBP1	glycosylphosphatidylinositol anchored high-density lipoprotein binding protein 1
h	hour(s)
H, His	histidine
H2O	water
HDL	high density lipoprotein
HEK	human embryonic kidney cells

HL	hepatic lipase
k_{cat}	rate of enzyme turnover
k_{cat}/K_M	catalytic efficiency
KCl	potassium chloride
KD	dissociation constant
kDa	kilodalton
K_i	dissociation constant for the inhibitor
K_M	Michaelis-Menten constant
L	liter
LDL	low-density lipoprotein
LDLR	low-density lipoprotein receptor
LMF1	lipase maturation factor 1
LPL	lipoprotein lipase
LRP	lipoprotein related-receptor protein
mg	milligram
$MgCl_2$	magnesium chloride
min	minute
mL	milliliter
mM	millimolar
N-terminal	amino terminal
NaCl	sodium chloride
Ni	nickel
$Ni2^+$	nickel cation

NIH	National Institutes of Health
nM	nanomolar
nm	nanometer
OD_{600}	optical density at 600 nm wavelength
oligos	oligonucleotides
p	p-value
PAGE	polyacrylamide gel
PBS	phosphate buffered saline
PCR	polymerase chain reaction
PDB	Protein Data Bank
pH	negative log (base 10) of the molar concentration of hydronium ions
PL	pancreatic lipase
PCSK9	proprotein convertase substilisin/kexin type 9
R0	Förster radius
r	interfluorophore distance
SDS	sodium dodecyl sulfate
SEM	standard error of mean
SmTIRF	single molecule total-internal reflection fluorescence
SPR	surface plasmon resonance
TAMRA	tetramethylrhodamine
TCEP	tris(2-carboxyethyl)phosphine
TG	triglyceride
TIRF	total-internal reflection fluorescence

Tris	tris(hydroxymethyl)aminomethane
TRLs	triglyceride rich lipoproteins
UNC	University of North Carolina at Chapel Hill
UNC-CH	University of North Carolina at Chapel Hill
VLDL	very low density lipoprotein
V5	GKPIPNPLLGLDST
Vmax	maximum velocity
WT	wild type
λ	wavelength
µg	microgram
µL	microliter
µM	micromolar
µm	micrometer

CHAPTER 1: INTRODUCTION TO LIPOPROTEIN LIPASE

Biological Function of Lipoprotein Lipase

Cardiovascular disease (CVD) is the leading cause of death both in the United States of America, and worldwide. Risk factors for developing CVD include smoking, physical inactivity, diet, metabolic syndromes such as diabetes, and blood lipids levels. In addition to high cholesterol, sustained high triglyceride (TG) levels in the blood are also an identified marker of increased CVD risk(1).

High circulating levels of TG often result from environmental factors, such as diet. In rare cases they can result from genetic mutations resulting in loss of lipoprotein lipase (LPL) activity. LPL is the rate-limiting enzyme responsible for hydrolysis of TGs from circulating TG-rich lipoproteins (TRLs). LPL also serves a lesser recognized role as a catalyst for the uptake of lipoproteins from the blood into the liver(2-5).

Genetic mutations leading to diminished LPL function lead to severe hypertriglyceridemia. LPL deficiency not only results from over 100 known LPL mutations(6), but also from genetic mutations in necessary LPL-interacting factors including lipase maturation factor 1 (Lmf1)(7), apolipoprotein CII (APOC-II), apolipoprotein AIV (APOA-V), and glycosylphosphatidylinositol anchored high-density lipoprotein binding protein 1 (GPIHBP1)(8).

Description of LPL Structure/Function

LPL is a 55 kDa secreted lipase that is active as a head-to-tail homodimer(9).

Lipases are serine-hydrolases classified as such based on their requirement for

interfacial activation. Interfacial activation occurs when an enzyme is most active at

an interface between lipid and water.

LPL belongs to the lipase gene family, a group of sequence similar secreted

lipases. Of these proteins, endothelial lipase (EL), hepatic lipase (HL), and LPL are

dimeric. The fourth member of the family, pancreatic lipase (PL) is monomeric, but

functions with the assistance of colipase(10-13). While no experimental x-ray

structure for LPL exists, PL is 30% identical and therefore provides a good homology

model for LPL.

Figure 1.1 shows a model of LPL generated using I-TASSER(14-17). Known,

functionally important domains of the protein are highlighted. LPL is comprised of

two major domains, linked by a small linker region. LPL's C-terminus is primarily a

regulatory domain comprised of beta-sheets. Several binding sites for LPL's

interacting partners have been identified within the C-terminus, including heparin

sulfates, GPIHBP1(18), and lipoprotein receptor-related protein (LRP) (5,19). In

addition, several tryptophan residues that are critical for lipoprotein binding are

clustered within LPL's C-terminus(20).

LPL's N-terminal domain contains the catalytic triad active site which is

covered by a helical loop termed the "lid". Lipase lids often move in response to

interfacial activation. For LPL, the lid is especially important for hydrolysis of long-

chain triglycerides(21) and mediating substrate specificity for triglycerides versus phospholipids(22,23). It has been shown that several tryptophans on LPL's C-terminus mediate substrate binding for the opposite monomer's active site(24). Specifically, the ability of one LPL oligomer to hydrolyze long-chain TG substrates is dependent on the intact lipoprotein binding domain of the other. Short-chain substrates are not restricted by lipoprotein binding, nor by replacement of LPL's lid by a short linker(24,25). These findings suggest that LPL's lid is not necessary for proper LPL catalysis of all substrates.

LPL's Regulation by Interaction Factors

Proper utilization of energy (fats and sugars) is critical to maintaining homeostasis during fasting, feeding, and exercise. Maintaining stable, yet healthy, levels of fat in lipoproteins circulating in the blood provides the body with energy on demand, and requires tight regulation of LPL. Further, LPL is an unstable protein that relies on many interacting partners to maintain activity *in vivo and in vitro.* As shown in Figure 1.2, the different types of LPL-interacting factor interactions can be classified as LPL processing, binding/stabilization, inactivation, and activation.

Posttranslational Control of LPL Folding and Secretion

Following translation, LPL requires the assistance of a special chaperone, LMF1 for proper folding and secretion from the endoplasmic reticulum(7,26,27). LPL has ten cysteine residues, all of which are contained in five required disulfide bonds, and two sites for glycosylation of N43(28) and N359 which are required for proper

3

LPL processing. The precise mechanism by which LMF1 controls the LPL folding process is ongoing work in the Neher Lab, but we believe that LMF1 plays a role in supporting quality control for proper LPL folding.

Following proper glycan trimming the Golgi, LPL is secreted into the interstitial space from where it is then translocated to the capillary lumen by GPIHBP1(8). GPIHBP1 has binding sites for both LPL and lipoproteins and therefore likely helps LPL come in contact with its substrates.

LPL Activation

The surface's of lipoproteins are decorated with apolipoproteins, which regulate LPL activity, lipoprotein uptake, and a variety of other functions, including many which are not well characterized. Among the apolipoproteins, loss of function of either APOC-II or APOA-V have been identified to result in a phenotype similar to LPL deficiency. This phenotype could be caused by either the apolipoproteins catalyzing LPL activity or lipoprotein uptake (29-31).

Intriguingly, while APOC-II is fairly abundant on the surface of lipoproteins, APOA-V is present in circulation at sub-lipoprotein levels (32). APOA-V has been poorly studied, but one report suggests that APOA-V is a poor activator of LPL and might instead assist in triglyceride turnover by bridging the interaction between surface bound LPL and lipoproteins(31). In contrast, studies suggest that APOC-II directly activates LPL(33).

Previous reports show that APOC-II increases the V_{MAX} of LPL(33). An interaction between the N-terminus of LPL (34,35) and a portion of APOC-II(35) has

been identified. One group has used the activating portion of APOC-II to develop

APOC-II mimetic peptides that are capable of rescuing APOC-II deficiency in

mice(36), however, no therapies are currently approved for APOA-V or APOC-II

deficiency in humans.

LPL Inactivating Factors

In addition to the apolipoproteins that activate LPL, apolipoprotein C1 (APOC-

I) and C3 (APOC-III) are also known to inhibit LPL (37-41) as well as another family,

of secreted macromolecular inhibitors, angiopoietin-like proteins (ANGPTL) 3, 4, and

8 (37,42). Like APOC-II and APOA-V, these inhibitors likely function by inhibiting

LPL catalysis, lipoprotein binding and/or uptake.

APOC-I and APOC-III both are capable of inhibiting LPL *in vitro* on

lipoprotein-like particles(40). It was recently shown that these apolipoproteins

displace LPL from the surface of lipoproteins(41), and thus reduce LPL mediated

lipoprotein receptor uptake, leading to increased circulating lipoproteins. Thus,

instead of inhibiting LPL, their mode of action is primarily believed to be through

inhibiting lipoprotein uptake into the liver(39).

APOC-I was also reported to inhibit lipoprotein binding to LRP in an LPL

independent fashion(39). Further, APOC-I has been shown to prevent free fatty acid

(FFA) esterification and uptake into cells (43). APOC-I knockout mice however did

not benefit from cardioprotective phenotypes(44), and thus APOC-I has not yet been

a target for TG lowering therapeutics.

APOC-III was found to be a more potent inhibitor than APOC-I(40) and has been a recent target for therapeutics. Volanesorsen is an antisense therapeutic oligonucleotide that targets APOC-III mRNA, and it is currently in phase three clinical trials(45,46). This treatment works by lowering APOC-III plasma concentrations, which has been successful in decreasing circulating TG levels.

The ANGPTL family of proteins are tissue-specific regulators of LPL activity that are known to directly inhibit LPL activity. Loss of either ANGPTL 3 or 4 results in low plasma triglyceride levels in mice(47,48), but not ANGPTL8(49). ANGPTL8(50) is the newest member of the ANGPTL family, and it is believed to require ANGPTL3 for activation, while ANGPTL3 can act alone to inhibit LPL(49,51). Antibodies reducing ANGPTL8 show reduced plasma triglycerides in mice(52), suggesting ANGPTL8 still plays a key role in LPL inhibition. ANGPTL4, however, is the most potent LPL inhibitor of the family and like LPL is found in the blood, and as a result, it is the best studied family member.

It was previously believed that ANGPTL4 inhibited LPL by acting as an unfolding chaperone, but our group found that ANGPTL4 inhibits LPL by acting as a reversible non-competitive inhibitor of LPL(53). Based on their high similarity and conservation of an LPL-inhibitory motif, the other members of the ANGPTL family likely inhibit LPL by a similar mechanism.

The finding that ANGPTL4 is a reversible inhibitor has paved the way for a new avenue of triglyceride lowering drugs aimed at disturbing the LPL/ANGPTL4 bond. The question of where ANGPTL4 binds and inhibits LPL *in* vivo remains an outstanding question that may prove critical for drug delivery. Drugs targeting the

LPL/ANGPTL4 interaction may require specific delivery to the plasma because ANGPTL4 is also believed to inhibit PL in the intestines(54). Inhibition of PL would be expected to increase fat adsorption into the intestine which in turn would increase circulating fat levels, but a previous study showed that carriers of loss-of-function ANGPTL4 mutations have a lower incidence of cardiovascular disease(55).

One group showed that LPL is protected from inhibition from ANGPTL3 and ANGPTL4 when LPL is bound to triglyceride rich lipoproteins(56), but conflicting data exists for inhibition of GPIHBP1 bound LPL. One study showed protection of LPL inhibition, by GPIHBP1, *in vitro*(57) while another showed that the addition of ANGPTL4 removes LPL from the outside of GPIHBP1 expressing cells in culture(58). Disruption of the LPL/GPIHBP1 interaction by ANGPTL4 suggests that an ANGPTL4 targeting therapeutic would need to target ANGPTL4 before it can disturb LPL on capillaries

Specific open research questions include how these protein inhibitors bind to LPL, how they affect its oligomeric state and if they cooperate to ensure appropriate physiological regulation of LPL's activity.

Therapeutic Strategies to Improve LPL Function

For patients suffering from severe hypertriglyceridemia due to familial lipase deficiency, a gene therapy drug, Alipogene Tiparvovec, is available in Europe(59). The LPL gene packaged in Alipogene Tiparvovec is for a slightly truncated version of LPL, LPL[S447X], which is the only characterized LPL gain-of-function mutation. Until recently, no mechanism for LPL[S447X]'s gain-of-function had been identified, although

several hypotheses have been tested. I have shown, as follows in the next chapter, that it is likely due to improved lipoprotein uptake(60). Improved lipoprotein uptake explains the striking difference in triglyceride levels seen in previous studies as each lipoprotein particle holds huge quantities of un-hydrolyzed triglycerides, so any small increase in uptake contributes greatly to TG clearance.

Alipogene Tiparvovec is the only approved therapy for LPL deficiency, only approved for use in Europe, and it only is suitable for patients with LPL gene perturbations, but not perturbations in genes such as APOC-II, APOA-V, LMF1, and GPIHBP1. Unfortunately, the million-dollar price-tag and reduced efficacy over a short period of time(61-63) make Alipogene Tiparvovec a poor option for treating LPL deficiency. While LPL deficiency due to homozygous mutation is relatively rare (<1%)(64), heterozygous LPL mutations that may reduce overall LPL function are fairly common and can contribute to increased CVD risk through reduced triglyceride hydrolysis and redistribution of smaller lipoproteins. To address impaired LPL function due to genetic and environmental factors, as well as in patients with high triglyceride levels not resolvable by current interventions, novel therapies are necessary.

Recent studies have focused on enhancing LPL activity by blocking its inhibition(45,65,66), activating catalysis(36,67), or stabilizing the enzyme(68). Despite the large number of known LPL regulatory proteins, the precise mechanisms by which many of these proteins interact with LPL, and their combined effects, require additional study. New methods to address these questions and to provide a

deeper understanding of LPL's function and structure would improve approaches to

target LPL with therapeutics.
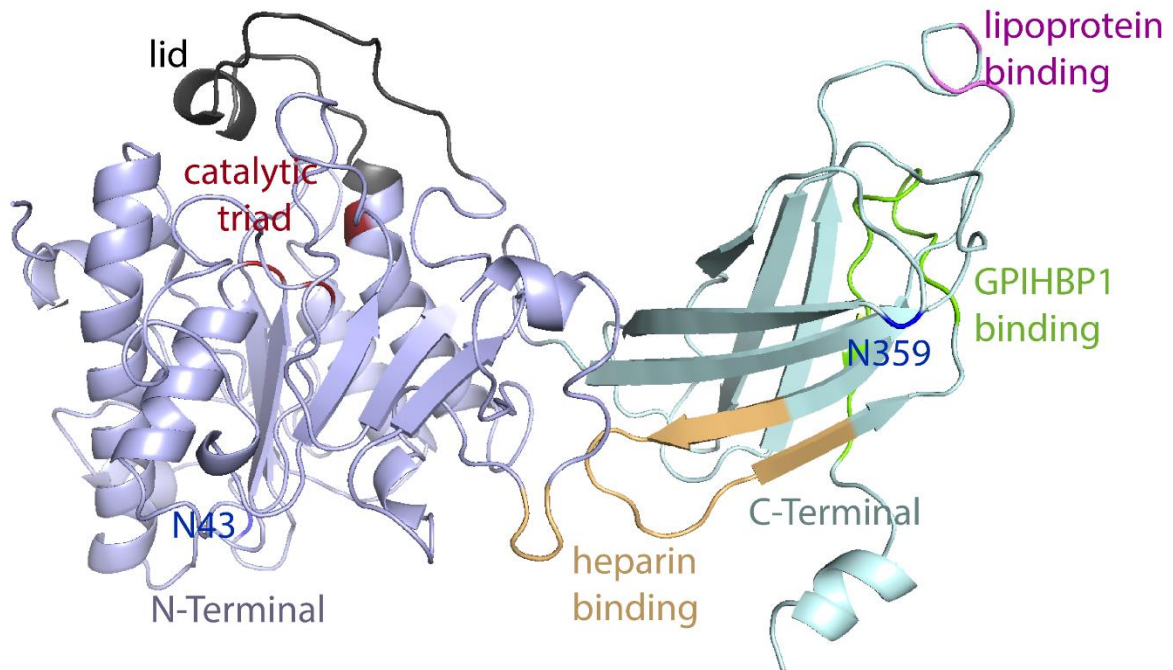
Figure 1.1 Structural Model of LPL

An I-TASSER(14-17) generated model of LPL threaded on the crystal structure of pancreatic lipase(10), a lipase with 30% sequence identity to LPL. LPL's N-terminus (light purple) contains the lid (dark grey), catalytic triad (dark red), N43 glycosylation site (blue), and a lower-affinity part of the heparin binding site. The C-terminal (light blue) contains LPL's heparin binding site (light orange), GPIHBP1 binding site (light green), lipoprotein binding patch (pink), and the N259 glycosylation site (blue).
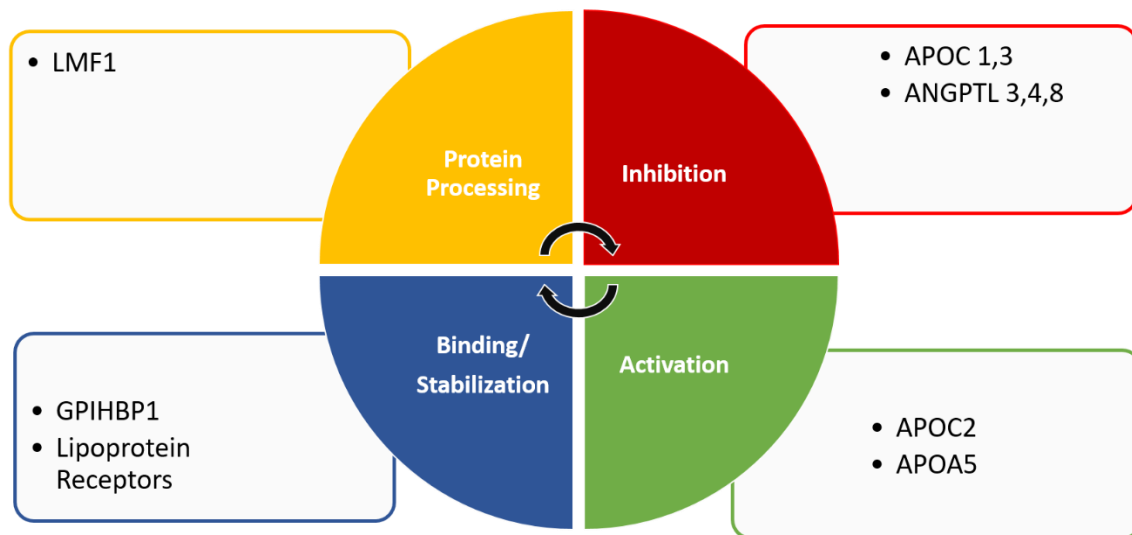
Figure 1.2 LPL is Highly Regulated by Different Groups of Interacting Proteins
LPL undergoes tight regulation through interaction with many protein partners.
Shown here is a diagram representing the different ways in which LPL interacting
partners are known to regulate its function.

CHAPTER 2: BIOCHEMICAL ANALYSIS OF THE LIPOPROTEIN LIPASE TRUNCATION VARIANT, LPL^{S447X}, REVEALS INCREASED LIPOPROTEIN UPTAKE[1]

Introduction

Nearly one third of the American population has elevated triglyceride (TG) levels, leading to increased risk for cardiovascular disease(69). Lipoprotein lipase (LPL), an obligate homodimeric enzyme, is the primary enzyme responsible for hydrolysis of circulating TG-rich lipoproteins. Although most identified mutations in the LPL gene are deleterious, one mutation, LPL^{S447X}, has been reported as a gain-of-function mutation(70). LPL^{S447X} is truncated by two amino acids at the C-terminus, which results in the loss of a serine and glycine. Intriguingly, studies comparing human LPL^{S447X} carriers to non-carriers report that carriers have a reduced incidence of myocardial infarction, and a favorable lipid profile highlighted by decreased TG and increased HDL(71-73). An analysis of LPL^{S447X} carriers who participated in the Framingham Heart Study found that approximately 17% of the American population carries at least one copy of the truncated LPL. Additionally,

---

male carriers showed an average of 13.8% reduction in TG levels whereas female carriers do not show changes in TG levels(72). Average TG reduction varies by study, and some studies identify female carrier populations with reduced TG levels(71).

Results from mouse studies were similar. LPL$^{-/-}$ mice rescued by retroviral treatment with LPL^{S447X} showed significantly lower triglyceride levels than LPL$^{-/-}$ mice treated with LPL(74). In that study, LPL^{S447X} and LPL protein levels did not significantly differ, whereas the activity of LPL^{S447X} was two times that of LPL. Despite the strong *in vivo* evidence from both mice and humans demonstrating that LPL^{S447X} is a gain-of-function mutation, the precise mechanism by which LPL^{S447X} is beneficial remains unclear. Past studies have compared the production, stability, and activity of LPL^{S447X} and LPL and cannot explain the *in vivo* phenomena(74-76).

In contrast to the *in vivo* studies, *in vitro* reports vary as to whether the LPL variants have different activity. Measurements of proteins in tissue culture media showed that LPL^{S447X} had increased(77), decreased(76,78), or no difference(79,80) in activity. Many of these studies used LPL quantified by ELISA to determine protein mass, whereas others use Western blots. These methods do not account for the inactive pools of LPL, which comprise the majority of the protein in media. Inactive LPL includes LPL that has undergone cleavage by proprotein convertases and monomeric LPL that can no longer dimerize(21,81). Further, the studies evaluated LPL's catalytic activity on non-physiological substrates, rather than on TG-rich lipoproteins.

One explanation for LPL^{S447X}'s observed *in vivo* gain-of-function could be changes in binding affinity between LPL and one or more of its interacting factors. Glycosylphosphatidylinositol anchored high-density lipoprotein binding protein 1 (GPIHBP1)(18) and lipoprotein receptor-related protein (LRP)(19) are both known to interact with the C-terminus of LPL, and could thus interact differently with LPL^{S447X}. GPIHBP1 is the protein responsible for translocation of LPL to the capillary lumen, and a recent study showed that its binding affinity for LPL^{S447X} was not altered, which suggests another factor may be the key to the difference(8,79). LRP is a receptor for the endocytosis of ApoE-containing lipoproteins, and LPL enhances LRP-mediated lipoprotein uptake(2,82,83). In support of this idea, a previous report by one group indicates an increase in clearance of lipoproteins in LPL^{S447X} carriers(84). We thus investigated the possibility that the benefits of LPL^{S447X} are not linked to enzymatic activity, but instead in how LPL bridges lipoprotein uptake.

An alternate explanation for enhanced LPL^{S447X} function is differences in how the two LPL variants are regulated by circulating activating and inactivating factors. Angiopoietin-like protein 4 (ANGPTL4) and apolipoproteins regulate LPL, but the specific binding sites on LPL are not known. We recently showed that ANGPTL4 inhibits LPL by a non-competitive mechanism(53). Because the ANGPTL4-binding region(s) on LPL are unknown, we hypothesized that ANGPTL4 might have decreased binding to the truncated variant of LPL, which would allow LPL to be more active *in vivo*. Alternatively, other alterations in binding may occur between LPL and the apolipoproteins that reside on the surface of lipoproteins. Thus,

LPL^{S447X} would have altered activity *in vivo* because key binding partners are present.

Here, we aim to understand the advantageous characteristics of LPL^{S447X} observed *in vivo* using biochemical assays to compare LPL and LPL^{S447X} activity alone and in the presence of various binding partners. We find that LPL and LPL^{S447X} have identical catalytic activity on artificial and natural substrates. We did not find a significant difference in ANGPTL4 inhibition of LPL, either in the presence or absence of GPIHBP1. Finally, we did see a difference in LPL-enhanced uptake of lipoproteins by hepatic cells. Modeling the LPL^{S447X} truncation onto the LPL structure suggests that loss of these two amino acids may provide enhanced access to the LRP receptor-binding site on LPL, which may also be where other lipoprotein uptake receptors bind to LPL. In keeping with this hypothesis, we found that LPL^{S447X} bound more tightly than LPL to the low-density lipoprotein receptor (LDLR).

Materials and Methods

Molecular Cloning

LPL and GPIHBP1 variants were cloned into pCDNA5/FRT/TO (Thermo Fisher Scientific). The human and mouse GPIHBP1 constructs included a HIS-tag after the cleavage sites, after amino acids 151 and 181, respectively. The cloning of pET16B_ANGPTL was previously described(53).

Protein Expression and Purification

LPL and GPIHBP1 expression and secretion were induced by replacing the growth medium with in Dulbecco's Modified Eagle Medium (DMEM) containing 1% Fetal Bovine Serum, 1% Penicillin-Streptomycin, and 1 mM L-Glutamine, with 20 μg/mL Tetracycline. For LPL, 10 units/mL Heparin and 1 mM $CaCl_2$ were also added.

LPL was purified over a HiTrap Heparin Sepharose High Performance Column (GE Healthcare Life Sciences), washed with 75 column volumes of 850 mM NaCl, 10% glycerol, 20 mM Bis-Tris pH 6.5 and eluted with 1500 mM NaCl, 10% glycerol, 20 mM Bis-Tris pH 6.5. Protein was concentrated, aliquoted, flash frozen in liquid nitrogen, and stored at -80° C until use. For GPIHBP1, the media pH was adjusted to >8.0. Media was then incubated with cOmplete His-Tag Purification Resin (Roche), washed with buffer (200 mM NaCl, 20 mM Tris 8.0), and eluted with buffer + 500 mM Imidazole. ANGPTL4 was purified as previously described(53).

Quantification of LPL Variants

Bovine LPL of a known concentration, purified as described(85), was used as a standard for the quantification of LPL variants. Bovine LPL and the LPL variants were incubated for 30 minutes at room temperature with an excess of ActivX TAMRA-FP Serine Hydrolase Probe (Thermo Fisher Scientific). Reactions were quenched by the addition of loading dye. Samples were loaded onto 12% gels and separated by SDS-PAGE. The gel was imaged using a Typhoon Trio+ imager (excitation 532 nm, 580 nm BP 30 emission filter, GE Healthcare Life Sciences).

ImageQuant TL software was used to quantify band intensities. Concentrations of the LPL samples (dimers) were calculated from the bovine LPL standard curve. Only unknown concentrations that fell within standard curves with $R^2 \geq 0.95$ were used in activity assays. Samples were quantified in triplicate. The LPL antibody α-4-1a, a kind gift from André Bensadoun, was used to demonstrate that the active-site labeled protein concentrations were equal to the purified dimer protein concentration(86).

Activity Assays for LPL, Using a Fluorescent Lipase Substrate

Activity assays were carried out essentially as described(53), except that 2.5 nM LPL was used, assays were carried out at 37 °C, and the first 200 seconds of the reaction was used to calculate the initial velocity. Deoxycholate (at 1 mM) was included in all reactions to stabilize LPL.

Activity Assays for LPL, Using Plasma-Derived Triglycerides

Plasma from patients with normal lipid profiles and hyperlipidemia were supplied by Dr. John Kane and were collected under protocol # 10-00272 as approved by the Institutional Review Board at the University of California at San Francisco. Informed consent was obtained from all human subjects. Triglyceride rich lipoproteins (TRLs) were isolated as previously described(87). TRLs were quantified as previously reported(88). 2.5 nM LPL, final concentration, was incubated with isolated lipoproteins in a volume of 30 μL. Individual reactions were quenched at 0, 3, 6, and 9 minutes by the addition 10 μL Orlistat (Cayman Chemical Company, Ann

Arbor, Michigan, USA) to a final concentration of 150 µM Orlistat in 40 µL. Released

free fatty acids (FFA) were quantified using reagents previously described(88). Initial

velocities were calculated by plotting FFA (µM) release against time from 0-9

minutes. Initial velocities were plotted as a function of substrate concentration and fit

to the Michaelis–Menten equation using Kaleidagraph to calculate the kinetic

parameters V_{max} and K_M. Each LPL sample was assayed at least five times.

Inhibition of LPL by ANGPTL4

To determine the K_i for ANGPTL4 inhibition of LPL, ANGPTL4 was added to

dilute LPL at a final volume of 70 µL/reaction. The reaction was initiated by the

addition of 30 µL of varying levels of DGGR in Anzergent (Affymetrix), to a final

volume of 100 µL. Samples were shaken in a Spectromax M5 plate reader, set to

37 °C, for 5 seconds and then substrate hydrolysis was measured by fluorescence

excitation at 529 nM, emission at 600 nM, and a filter of 590 nM. Final assay buffer

concentrations were 150 mM NaCl, 1 mM deoxycholate, 20 mM Tris pH 8.0, 0.2 %

Fatty Acid Free BSA, and 0.01 % Anzergent. Final ANGPTL4 concentrations were 0,

0.25, 0.5, 1.0, and 2.0 µM. The rate of initial LPL substrate hydrolysis was plotted as

a function of substrate concentration. Next, data were fit to the equation for

noncompetitive inhibition: $v = V_{max}*[S]/\{(K_M*(1+[I]/K_i))+([S]*(1+[I]/K_i))\}$ where V_{max} is

the uninhibited maximum rate of substrate hydrolysis, K_M is the Michaelis-Menten

constant, [S] is substrate concentration, [I] is inhibitor concentration, and K_i is the

inhibition constant. Data were fit using simultaneous nonlinear regression with the

program Mathematica (Wolfram Research).

ANGPTL4 Inhibition in the Presence of GPIHBP1

LPL assays were conducted essentially as described above for the LPL activity assays, without the inclusion of deoxycholate because GPIHPBI stabilizes LPL. GPIHBP1 (approximately 80 nM final concentration) was pre-incubated with LPL diluted in assay buffer before the addition of ANGPTL4 (0.5, 1.0 and 2.0 μM final concentration).

Measurement of Low-Density Lipoprotein Uptake

Clear bottom, black sided 96-well plates were coated with 0.1 mg/mL Poly-D-Lysine and allowed to incubate for 8 minutes. Wells were then washed three times with PBS and the plates were cured under UV light for at least 15 minutes. Alternatively, TC-treated 96-well black sided, clear bottom plates were used. HepG2 cells were seeded and allowed to grow to approximately 90% confluence in DMEM containing 10% Fetal Bovine Serum, 1% Penicillin-Streptomycin, and 1 mM L-Glutamine. Cells were starved for 2.5 hrs in Phosphate Buffered Saline (PBS), and then the PBS was replaced with PBS with or without 10 nM LPL (desalted into PBS) and 1X LDL-550 (Abcam). Cells were incubated for 30 minutes then washed three times with PBS. 50 μL fresh PBS was added to the cells and wells were read for fluorescence intensity at 570 nm after excitation with a laser at 540 nm. Each plate contained at least triplicate wells for control, LPL, and LPL[S447X] samples. Data from different days was consistent, but to account for small deviations in cell number, confluency, and time, samples were normalized to the LDL alone control measured each day. Experiments were conducted on three different days.

Measurement of Very-Low-Density Lipoprotein Uptake

Huh-7 cells were seeded into TC-treated 96-well black sided, clear bottom plates and allowed to grow to near confluence in DMEM containing 10% Fetal Bovine Serum, 1% Penicillin-Streptomycin, and 1 mM L-Glutamine. Cells were starved for 2 hours in PBS, and then the PBS was replaced with PBS with or without 20 nM LPL (desalted into PBS) and fluorescently labelled VLDL. VLDL was labelled as previously described(89), except 1,2-dioleoyl-sn-glycero-3-phosphoethanolamine-N-(carboxyfluorescein) salt (Avanti) was used for the labeling reagent. Cells were incubated with LPL/VLDL mixtures for 30 minutes then washed three times with PBS. Fresh PBS was added to the cells and the fluorescence was measured by excitation at 494 nM, emission at 515 nM, and a cut-off filter at 515 nM. Each plate contained at least four wells per sample, controls, LPL, and LPL[S447X] samples. Data from different days was consistent, but to account for small deviations in cell number, confluency, and time, samples were normalized to the LDL alone control measured each day. Experiments were conducted on three different days.

LPL Modelling

Lipoprotein lipase was modeled using the I-TASSER structure prediction server(14,16,17). Top threading templates used included human pancreatic lipase (2PPL) and horse pancreatic lipase (1HPL). All templates were between 28-30% sequence identity and greater than 93% sequence coverage. Despite the high sequence coverage, the c-terminal tail residues of LPL (439-448) are not homologous to any of the threading templates used by I-TASSER. To further model

the C-terminal tail of LPL, the FloppyTail application within the Rosetta software suite was used to determine 1100 possible structural conformations for residues 439-448(90). The top 10 lowest energy structures (Figure 2.1) were analyzed to identify feasible interactions between the C-terminal tail and regions of LPL known to play a role in receptor binding.

Analysis of LPL LDR Binding by SPR

SPR experiments were performed using the ProteOn XPR36 (Biorad) with the HTG Sensor Chip and Kit (Biorad). His-tagged LDLR (Invitrogen) was immobilized on the chip by flow at 25 µL/min for 120 seconds. Buffer blanks were taken for 60 seconds at 100 µL/min. Finally, LPL variants at 6.6 and 20 nM were flowed over channels with or without LDLR for 100 seconds at 100 µL/min. All measurements were carried out at 25 °C in 50 mM Tris 8.0, 400 mM NaCl, 1% glycerol, 0.005 % Tween-20, 2 mg/mL BSA, 2 mM $CaCl_2$, and 1 mM deoxycholate. All data was collected and analyzed using ProteOn Manager. Buffer and a channel with no LDLR were background subtracted from the data. A Langmuir interaction model for 1:1 binding with simultaneous on/off was used to estimate kinetic parameters.

Results

LPL and LPLS447X are Equally Active on Natural and Synthetic Substrates

LPL[S447X] could show a gain-of-function phenotype *in vivo* because it has a higher specific activity than LPL. We thus set out to determine if the LPL variants differ in their specific activities using the purified, dimeric fraction of both LPL and

LPL^{S447X}. We precisely quantified the amount of active lipase in each preparation using an activity based probe(91), which fluorescently labels the active site serine of only properly folded, active lipases (Figure 2.2A). We next analyzed lipase activity using DGGR, a synthetic substrate that produces a fluorescent signal upon hydrolysis. Equal amounts of LPL and LPL^{S447X} were assayed at increasing substrate concentrations to complete a full Michaelis–Menten curve. As shown in Table 1 and Figure 2.2B and C, LPL and LPL^{S447X} showed no difference in V_{max} or K_M when assayed on DGGR. Thus, from these quantitative kinetic assays using purified, precisely quantified LPL variants, LPL^{S447X} does not have an enhanced ability to bind or hydrolyze substrate relative to LPL.

Because LPL^{S447X} and LPL showed similar specific activity on a synthetic substrate, we asked if LPL^{S447X} had enhanced triglyceride hydrolysis activity on a natural substrate. Lipoproteins contain apolipoproteins that alter LPL activity. For example, APOC-II, a component of VLDL and chylomicrons, activates LPL, whereas APOC-III inhibits LPL(37). We thus tested the hypothesis that LPL^{S447X} could be more activated or less inhibited than LPL by an apolipoprotein component of its natural substrates. Chylomicrons from a patient with severe hypertriglyceridemia were used to achieve maximal substrate concentration for a full Michaelis-Menten analysis. No difference in V_{max} or K_M between LPL and LPL^{S447X} was observed on chylomicrons (Table 2, Figure 2.3A). In addition, LPL^{S447X} and LPL showed identical activity on VLDL purified from a patient with a normal lipid profile (Figure 2.3B). Because the LPL variants are equally active on triglyceride rich lipoproteins (TRLs),

these data suggest that there is no difference in the interaction of the LPL variants with the apolipoproteins on the surface of the TRLs.

No Significant Difference in ANGPTL4 Inhibition of LPL vs. LPL^{S447X}

LPL activity is inhibited not only by APOC-III, but also by soluble secreted proteins including ANGPTL4. We thus measured the ANGPTL4 inhibition of both LPL variants. LPL activity was measured over several substrate concentrations in the presence of increasing amounts of ANGPTL4. Data were fit to an equation for noncompetitive inhibition. No significant difference in K_i was observed (*p*-value > 0.05, Figure 2.4), suggesting that ANGPTL4 does not inhibit LPL^{S447X} more than LPL.

No Difference in GPIHBP1-Mediated Protection of LPL vs. LPLS447X Against ANGPTL4 Inhibition

Because ANGPTL4 does not inhibit LPL^{S447X} to a greater extent than LPL, we wanted to determine if ANGPTL4 inhibited the two LPL variants differently in the presence of GPIHBP1. In a previous study, it was shown that soluble GPIHBP1 protects LPL from inhibition by ANGPLT4(57). Another study showed that ANGPTL4 displaces LPL from GPIHBP1(58). Although GPIHBP1 bound equivalently to LPL and LPL^{S447X}, it is possible that GPIHBP1 differently protects LPL and LPL^{S447X} from inhibition by ANGPTL4(79). We therefore tested the protective effect of GPIHBP1 on LPL and LPL^{S447X} inhibition by ANGPTL4. We tested LPL inhibition at three concentrations of ANGPTL4, one at and two above the K_i for inhibition of LPL.

Neither LPL variant was preferentially protected against ANGPTL4 inhibition (Figure 2.5). Thus, ANGPTL4 does not inhibit the two LPL variants differently, even in the presence of LPL's physiological binding partner, GPIHBP1. One unexpected outcome of these experiments was that we observed that only truncated mouse GPIHBP1, but not truncated human GPIHBP1, was secreted from cells in culture (Figure 2.6). Thus, mouse GPIHBP1 was used in these experiments.

LPL^{S447X} Enhances Lipoprotein Uptake to a Greater Extent that LPL

LPL is responsible for bridging the uptake of LDL and VLDL particles by the liver(2,92), through an interaction mediated by the C-terminus of LPL(19,93). We measured the ability of LPL and LPL^{S447X} to assist with LPL-mediated lipoprotein uptake. Accordingly, we incubated LDL particles conjugated to DyLight-550 with cultured HepG2 hepatic cells and measured the resulting fluorescence intensity of the cells. We observed that both LPL and LPL^{S447X} increased LDL uptake into the HepG2 cells. However, LPL^{S447X} increased LDL uptake more than LPL and this difference was significant (p-value < 0.05, Figure 2.7A). To further explore this result, we utilized SPR to analyze the interaction between the two LPL variants and the LDLRV. These experiments revealed that both LPL and LPL^{S447X} bound to LDLR with sub-nanomolar affinity, but LPL^{S447X} binding was several orders of magnitude tighter (Figure 2.8).

LPL^{S447X} also increased uptake of VLDL more than did LPL. To analyze uptake of fluorescently labeled VLDL, we used Huh-7 cells as we observed that VLDL uptake was more robust in these cells. Again, we observed that LPL^{S447X}

23

enhanced lipoprotein uptake relative to LPL, and this difference was significant
(Figure 2.7B, $p < 0.05$). Thus, our study suggests that the beneficial effect of LPL^{S447X}
stems at least partly from its ability to more greatly enhance the receptor-mediated
uptake of lipoproteins by the liver.

Discussion

The LPL^{S447X} mutation occurs in 10-20% of the population(94). It is different
from other rare and common LPL mutations in that it has a beneficial effect.
Although many theories have been proposed and tested, the precise reason that
loss of these last two amino acids enhances LPL's function is still unknown(71).
Despite this ambiguity, LPL^{S447X} is used in Alipogene tiparvovec (Glybera), the gene
therapy product for LPL deficiency(95). Use of LPL^{S447X} for gene therapy is
supported by a study in mice comparing rescue of LPL deficient mice with LPL vs.
LPL^{S447X} via adenoviral-mediated gene transfer(74). This study provided strong
evidence that LPL^{S447X} is a gain of function mutation and that the effect occurs at the
protein level because the two versions of LPL were expressed in identical adenoviral
vectors(74). Studies in humans and mice suggest that LPL levels in post-heparin
plasma are not different between LPL and LPL^{S447X} individuals(74,84,96). Other
studies note that any differences in plasma protein levels could be explained by the
use of different LPL antibodies (74). Thus, in the absence of significant differences in
plasma protein levels, LPL^{S447X} must either have intrinsically higher catalytic activity,
have a higher fraction of active LPL due to increased stability to inhibition, or it must

enhance hepatic uptake of lipoproteins from the blood. As discussed below, we provide biochemical evidence that favors the last explanation.

To date, data showing that LPL^{S447X} has enhanced catalytic activity have been contradictory, with studies showing that LPL^{S447X} has increased[77], decreased[78], or no difference[79,80] in activity. These disparate results are likely due to the fact that these studies used conditioned media as a source of LPL. These assays generally use unpurified LPL variants that are quantified via ELISA or Western blot. These methods for quantification do not account for the inactive monomeric and cleaved populations of LPL, which make up the majority of the protein population secreted into tissue culture media. We therefore purified human LPL and LPL^{S447X} from conditioned media using heparin-sepharose chromatography. We quantified the amount of *active* LPL using a fluorescent, activity-based protein probe that targets serine hydrolases[91]. We used the well-quantified, active LPL in measurements of the hydrolysis of the synthetic substrate DGGR. These data show that there is no difference in substrate binding or hydrolysis between the variants, nor two C-terminally tagged versions of LPL (data not shown). We also tested the idea that the kinetics of substrate binding and hydrolysis of LPL's natural substrates, TRLs, were different than the hydrolysis of the synthetic model substrate. LPL's natural substrates of TRLs are decorated with apolipoproteins that regulate LPL activity and particle uptake. Hydrolysis assays using TRLs isolated from human serum as substrates showed that LPL^{S447X} does not have significantly different hydrolytic activity than LPL. This finding is in agreement with our studies using a synthetic substrate, and indicates that there is no

25

difference in enzymatic activity between the two LPL variants. Furthermore, these findings suggest that the differences seen *in vivo* do not result from differences in the interactions of the LPL variants with lipoproteins during hydrolysis.

To examine the possibility that the differences between LPL[S447X] and LPL *in vivo* could be explained by LPL's interaction with one of its many regulatory factors, we tested inhibition by ANGPTL4 both alone and in the presence of GPIHBP1, which has been reported to protect LPL from ANGPTL4-mediated inhibition(57). LPL and LPL[S447X] bind to GPIHBP1 equivalently, although residues 421-435 in LPL's C-terminus mediate LPL binding to GPIHBP1(18,79). Therefore, the LPL[S447X] truncation could result in less LPL exposed when it is GPIHBP1-bound and thus better protection of LPL from inhibition. However, we did not find a significant difference in ANGPTL4 inhibition of the two LPL variants, either in the presence or absence of GPIHBP1.

Independent of its catalytic activity, LPL enhances the receptor-mediated uptake of lipoproteins via at least three receptors. LPL enhances the binding, uptake and degradation of triglyceride-rich and remnant lipoproteins mediated by the LRP(2,82). LPL also enhances the LDL receptor-mediated uptake of LDL particles(92), and enhances TRL uptake through the VLDL receptor (VLDLR)(97). Previous reports demonstrate that the C-terminal domain of LPL is responsible for the interaction with LRP(3-5,19,98). The specific domains of LPL that mediates interaction with the VLDL and LDL receptors are not yet known. Using fluorescently labeled LDL and VLDL particles, we found that liver-derived cells (HepG2 and Huh-7, respectively) took up more of the labeled lipoproteins when LPL[S447X] vs. LPL was

26

added. This result is due to enhanced receptor binding by LPL^{S447X}, rather than enhanced TRL binding, because both LPL variants had equivalent K$_M$ values for hydrolysis of TRLs. We also show that LPL^{S447X} binds to the LDLR more tightly than does LPL (Figure 2.8). Finally, our results are consistent with a study comparing APOB100 metabolism in individuals homozygous for LPL^{S447X} to control subjects, which showed that APOB100 LDL clearance was enhanced in homozygous LPL^{S447X} individuals(84).

Further, our findings make structural sense in light of a study by Chappell et al.(98) in which the C-terminus of LPL was expressed in *E. coli* and tested for its ability to enhance VLDL uptake. In that study, the authors found that four single point mutations in LPL (R405A, K407A, K413A, and K414A) are each sufficient to reduce the LPL-enhanced uptake of VLDL particles. Other groups suggest a similar LRP binding region on LPL involving residues 390-421(3), 313-448(5), or 380-425(4). In Figure 2.1, we modeled LPL's structure using I-TASSER(14,16,17). Because the C-terminal tail of LPL was not homologous to any of the threading templates used by I-TASSER, we further modeled it using the FloppyTail application within Rosetta(90). These models suggest that the LRP-binding region on LPL encompassing residues 405-414 (Figure 2.9, magenta) may be occluded by LPL's C-terminal tail (Figure 2.9, cyan and blue). In particular, amino acids 447 and 448, the amino acids lost in LPL^{S447X}, may contribute to binding interactions that stabilize interactions between the C-terminal tail and the LPR-binding region (Figure 2.10). We therefore suggest that the truncated version of LPL has improved uptake because it provides more access to the LRP-binding region of LPL between residues 405-414. It is possible

27

that LDLR, VLDLR, and LRP all bind to LPL in a similar fashion. LDLR and VLDLR share 46% sequence identity and both share homology with LRP through its many low density lipoprotein receptor class domain repeats.

LPL[S447X] has long been a mysterious gain-of-function mutation. Past experimental and population studies have produced contradictory results to explain why LPL[S447X] carriers benefit from a cardioprotective phenotype. Our intensive biochemical approach allows us to conclude that the cardioprotective effect of LPL[S447X] is not likely due to a difference in specific activity or interaction with apolipoproteins. We observed no significant changes in ANGPTL4 inhibition on LPL[S447X] as compared to LPL, indicating that changes in inhibition are unlikely the factor resulting in the changes seen *in vivo*. Rather, our data support the idea that LPL[S447X] increases LPL-mediated lipoprotein uptake. A model of LPL's structure suggests that when LPL's last two amino acids are lost, interactions between LPL's C-terminus and a region needed for uptake receptor binding are weakened. As a result, the receptor-binding region could be more exposed in LPL[S447X] as compared to LPL, resulting in enhanced receptor-mediated uptake of lipoproteins.
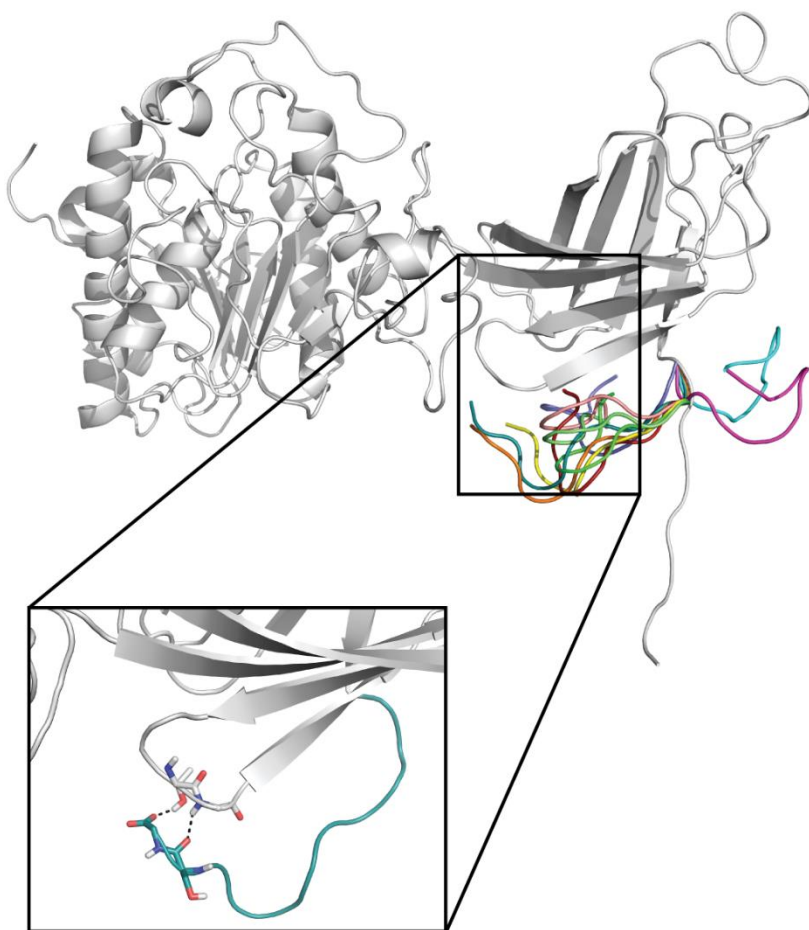
Figure 2.1. Ten Low-Energy Models of LPL's Tail as Predicted by Floppy-Tail.
A LPL homology model was predicted by I-TASSER and then modified to have an
extended tail and used as the starting structure for Rosetta:FloppyTail (gray).
Possible tail structures (colored) show that the C-terminus of LPL is proximal to
residues 405-414. Zoomed view shows feasible hydrogen binding interactions
between the backbone of residues 447 and 448 with the side chain of residue 411
and backbone of residue 412.
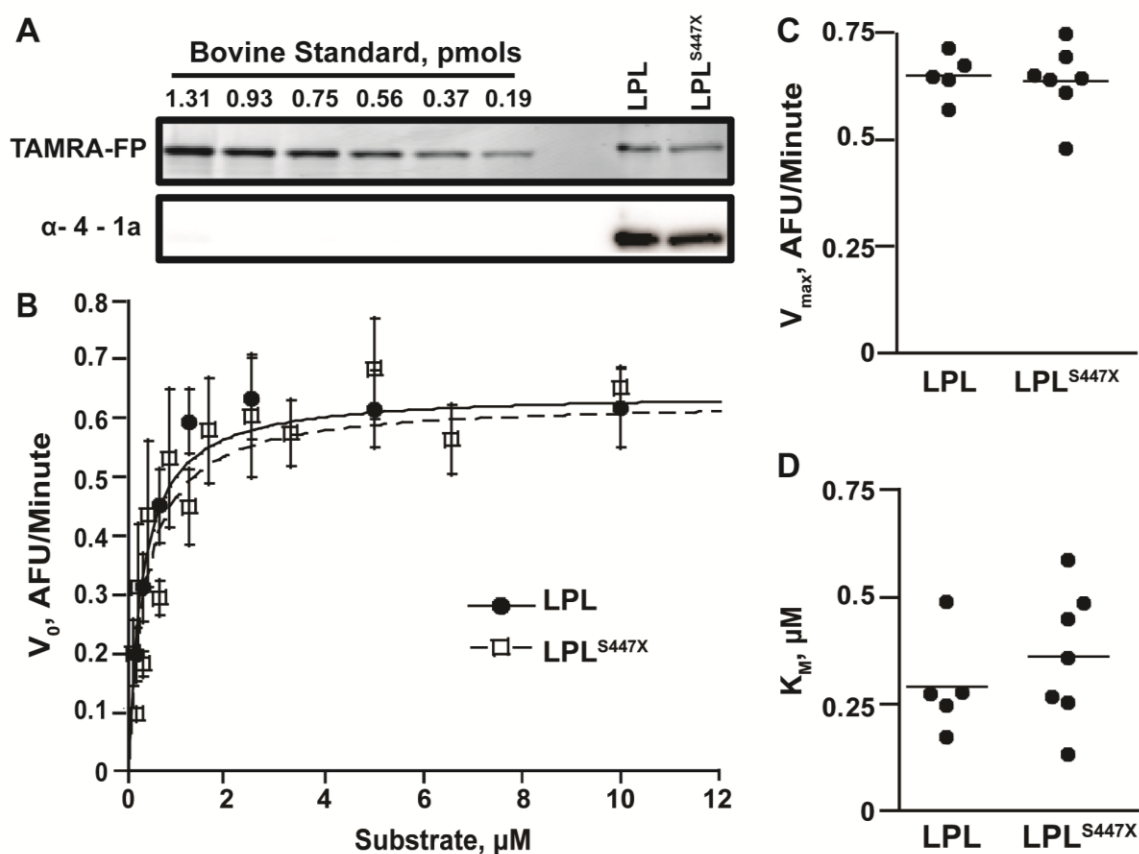
Figure 2.2. LPL and LPL[S447X] are Equally Active on the Lipase Substrate DGGR.
A) An activity based probe was used to quantify the amount of active human LPL and LPL[S447X] using bovine LPL as a standard. The equal concentration of LPL and LPL[S447X] is verified by Western blot using an antibody more sensitive to human LPL.
B) A Michaelis–Menten curves showing that LPL (filled circles) and LPL[S447X] (empty squares) have identical activity when hydrolyzing a synthetic substrate.
C) Graph of V_{max} and K_M values from multiple experiments for both LPL variants. A two-tailed student's *t*-test showed no significant difference in V_{max} ($p > 0.05$) and K_M ($p > 0.05$) for LPL vs. LPL[S447X].
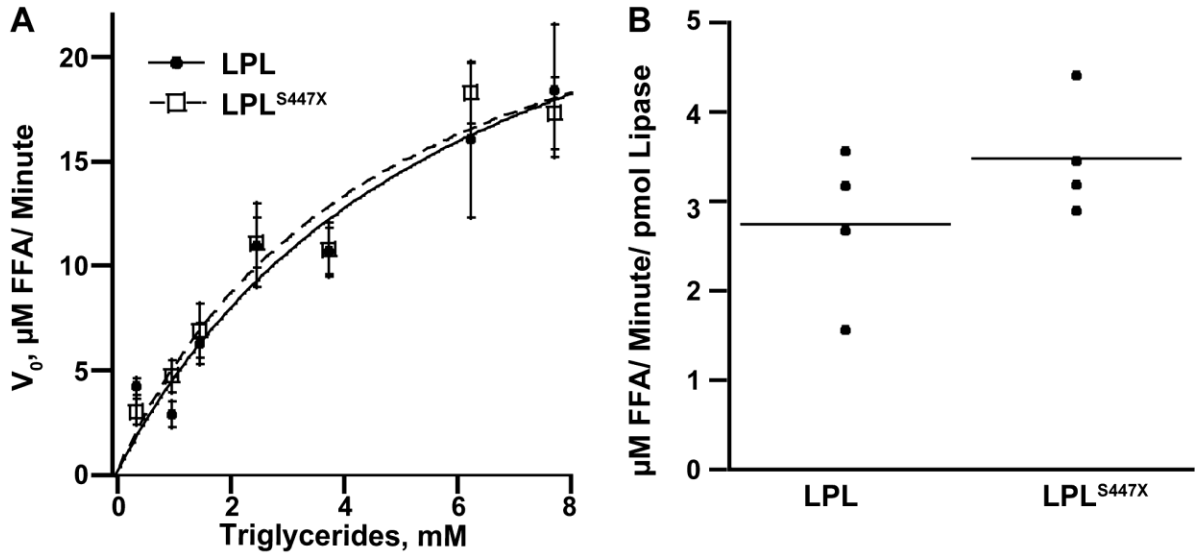
Figure 2.3. LPL and LPL^{S447X} Hydrolyze TRLs Equivalently.
A) Hydrolysis of chylomicrons by LPL and LPL^{S447X} **B)** Hydrolysis of VLDL by LPL and LPL^{S447X}. A two-tailed student's *t*-test showed no significant difference between LPL vs. LPL^{S447X} in the V_{max} ($p > 0.05$) and K_M ($p > 0.05$) on chylomicrons. There was not a significant difference between LPL vs. LPL^{S447X} hydrolysis of VLDL ($p > 0.05$).
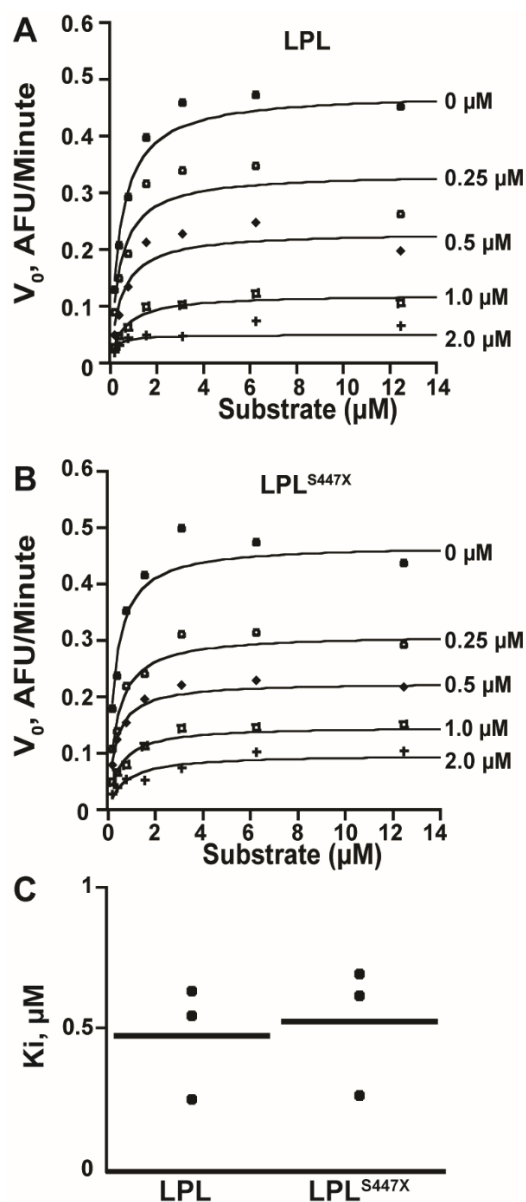
Figure 2.4. ANGPTL4 Inhibits LPL and LPL^{S447X} Equivalently.
Example Michaelis–Menten curves of **A**) LPL and **B**) LPL^{S447X} showing inhibition with increasing concentrations of ANGPTL4 over multiple substrate concentrations to obtain K_i values. Data was fit to an equation for noncompetitive inhibition. **C)** Data from independent experiments performed on different days with different ANGPTL4 preps is plotted. There is no significant difference in ANGPTL4 inhibition of LPL and LPL^{S447X} ($p > 0.05$).
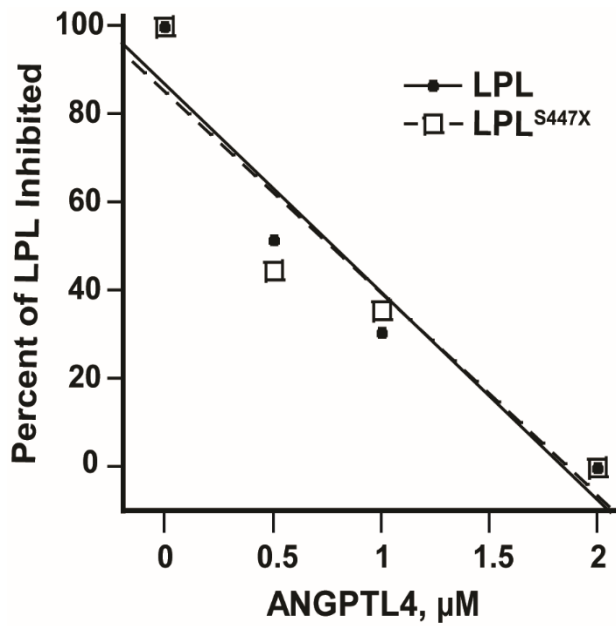
Figure 2.5. LPL and LPL^{S447X} are Equivalently Inhibited by ANGPTL4 in the Presence of GPIHBP1.

LPL and LPL^{S447X} were pre-incubation with GPIHBP1 and then increasing concentrations of ANGPTL4 were added, and LPL activity was tested. These experiments show that LPL and LPL^{S447X} are equivalently inhibited by ANGPTL4 in the presence of GPIHBP1.

33
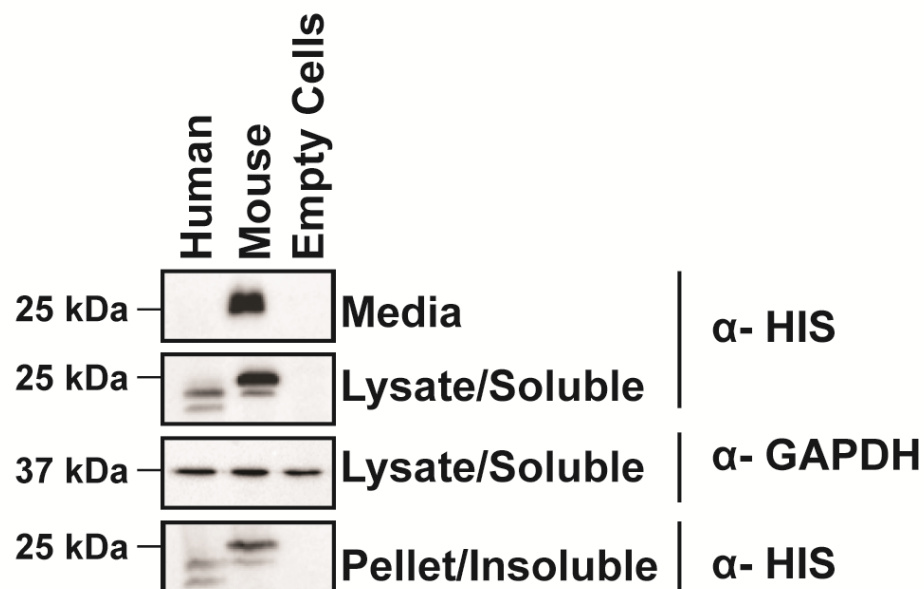
Figure 2.6 Mature Mouse, but Not Human GPIHBP1 is Secreted from Cells.
Stable cell lines containing HIS-tagged GPIHBP1 variants or regular HEK cells were
induced for protein expression. Media was collected and cells were lysed.
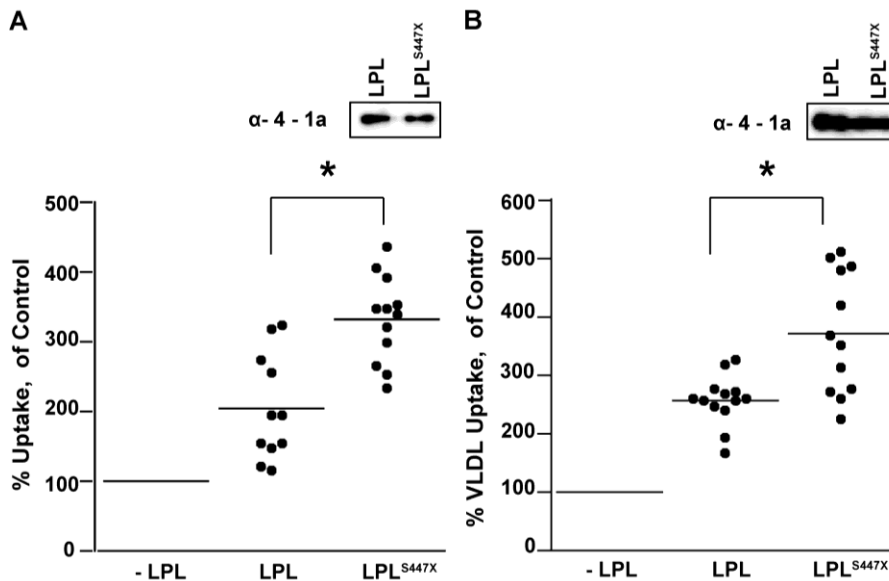
Figure 2.7. LPL^{S447X} Enhances Uptake of Fluorescent Lipoprotein Particles to a Greater Extent than LPL.

A) Uptake of DyLight-550 labeled LDL by HepG2 cells in the presence of LPL and LPL^{S447X}, as compared to no LPL. Randomly selected representative replicates from three different days are shown. A two-tailed student's *t*-test showed a significant difference in LDL uptake mediated by LPL vs. LPL^{S447X} ($p \ll 0.005$). Both variants showed a significant difference in uptake when compared to the control without LPL. B) Uptake of fluorescein labeled VLDL by Huh-7 cells in the presence of LPL and LPL^{S447X}, as compared to no LPL. A two-tailed student's *t*-test showed a significant difference in VLDL uptake mediated by LPL vs. LPL^{S447X} ($p < 0.005$). LPL loading is shown via anti-4-1a Western blot for both experiments.
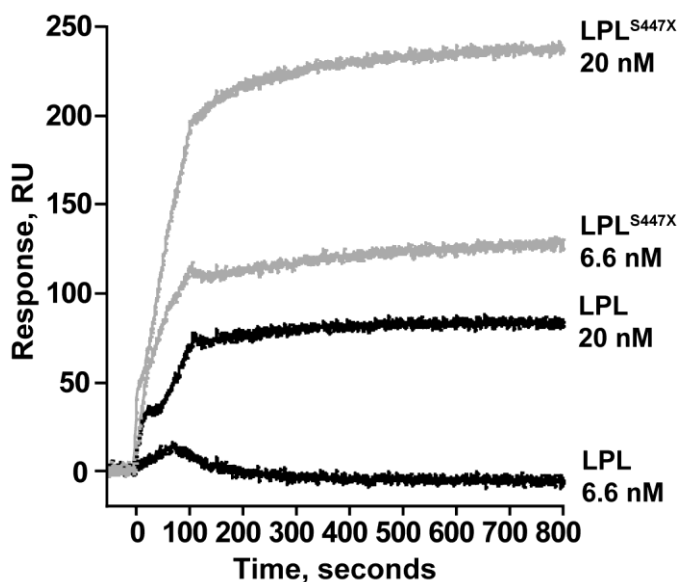
Figure 2.8. SPR reveals tighter binding of LPL^{S447X} to LDLR-HIS.
Binding of LPL (black lines) or LPL^{S447X} (grey lines), at indicated concentrations, to immobilized LDLR at was measured in 50 mM Tris 8.0, 400 mM NaCl, 1% glycerol, 0.005% Tween-20, 2 mg/mL BSA, 2 mM $CaCl_2$, and 1 mM deoxycholate at 25°C. Extremely tight binding to both LPL variants was evident by lack of significant dissociation, but differences in binding between the two proteins was evident.
The estimated K_D values were 6.16 x 10^{-10} M and 1.77 x 10^{-25} M for LPL and LPL^{S447X}, respectively; however, these values are only an estimate because the tight binding, as evidenced by lack of measurable dissociation, prevents accurate measurement of the binding parameters.
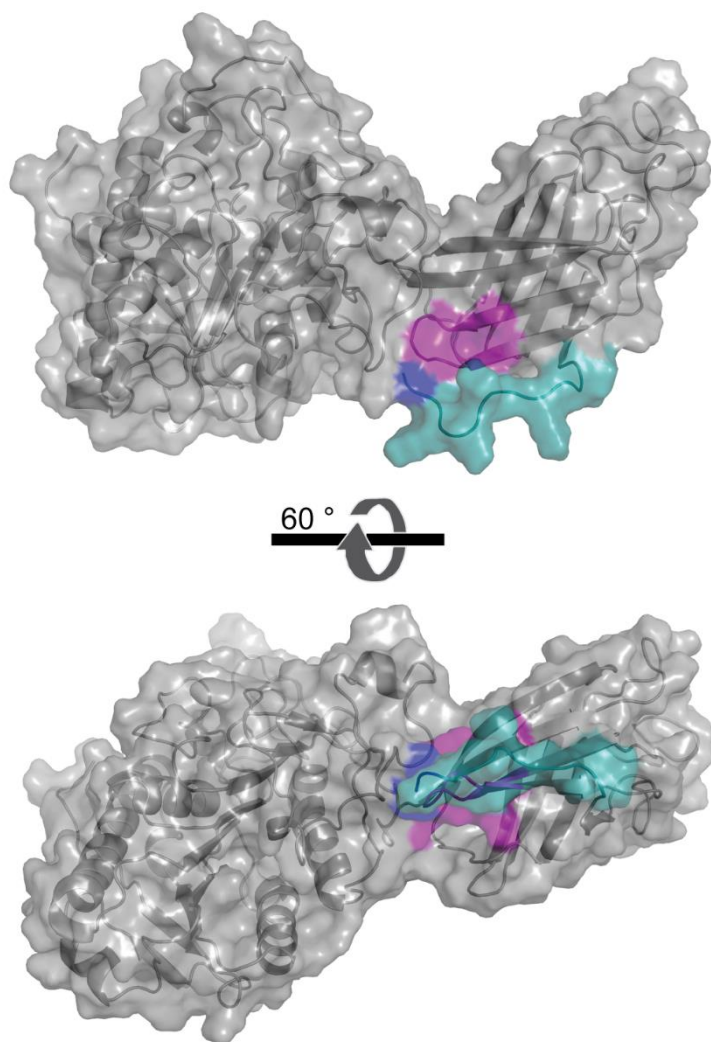
Figure 2.9. Potential Model for the LPL^S447X Gain-of-Function.
A homology model of LPL as predicted by I-TASSER was further refined using Rosetta:FloppyTail to find possible C-terminal tail confirmations. A low energy structure is shown in which the tail of LPL (439-448 colored in green/blue) occludes residues 405-414 (magenta). By this model, residues 447 and 448 (blue) can feasibly form hydrogen bonds with residues 411 and 412. Additional Rosetta:FloppyTail predicted models can be seen in Figure 2.9.
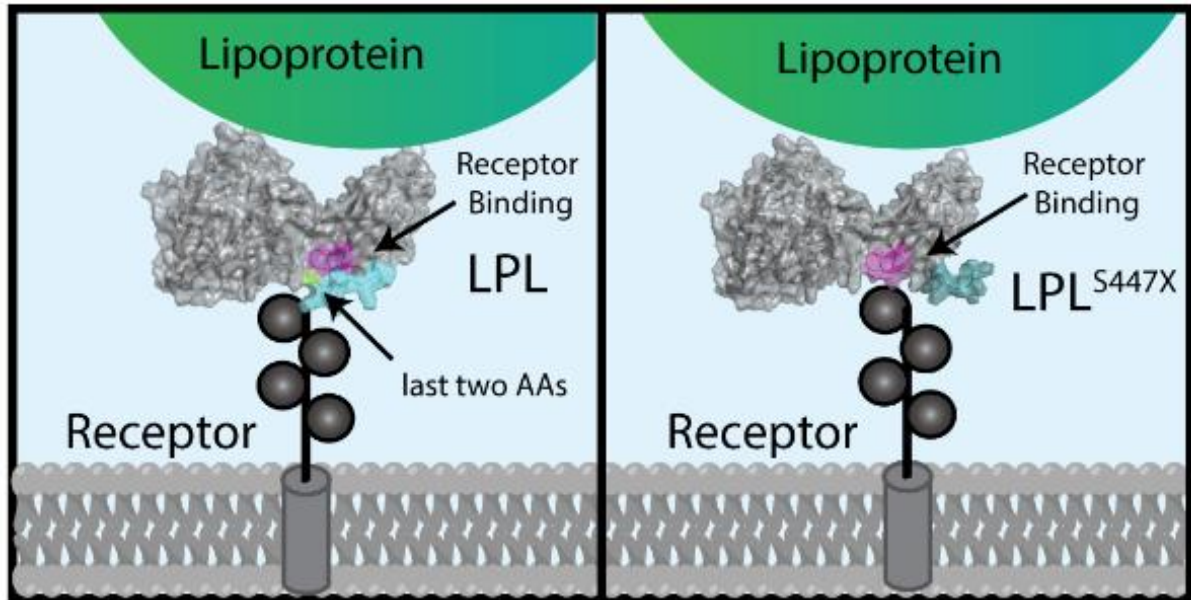
Figure 2.10. Model of LPL^S447X gain of function.
Removal of two amino acids for LPL's C-terminus results in improved uptake of lipoproteins possibly due to improved access to the known binding site for lipoprotein uptake receptors. This model shows wildtype on the left, and the improved access provided by amino acid removal, on the right.

Table 2.1. Activity of LPL Variants on DGGR

	V_{max} RFU/s	K_M M
LPL	$(10.82 \pm 1.00) \times 10^{-3}$	$(2.78 \pm 0.66) \times 10^{-7}$
LPL^{S447X}	$(10.32 \pm 1.41) \times 10^{-3}$	$(3.40 \pm 0.92) \times 10^{-7}$

Table 2.2. Activity of LPL Variants on Lipoproteins Isolated from Human Blood

	V_{max} (Chylomicrons) TG (M/s)	K_M (Chylomicrons) (M)	Rate (VLDL) FFA (M/s/mol lipase)
LPL	$(5.32 \pm 1.37) \times 10^{-4}$	$(6.09 \pm 2.82) \times 10^{-3}$	$(4.56 \pm 1.45) \times 10^{-2}$
LPL^{S447X}	$(4.83 \pm 0.09) \times 10^{-4}$	$(4.74 \pm 1.68) \times 10^{-3}$	$(5.80 \pm 1.10) \times 10^{-2}$

CHAPTER 3: SINGLE MOLECULE FLUORESCENCE IMAGING: A NEW APPROACH TO STUDY LIPOPROTEIN LIPASE DYNAMICS AND INTERACTIONS

Introduction

LPL is a useful therapeutic target not only for LPL deficient individuals, but also for the third of the American population that suffers from severe hypertriglyceridemia. For many Americans, intervention with available pharmaceuticals and lifestyle changes are not sufficient to lower circulating triglyceride levels. While Alipogene Tiparvovec is available in Europe for people with familial LPL deficiency, no therapies aimed at lowering triglycerides through modulating LPL are available outside of clinical trials.

Improving LPL stability and activity are both attractive targets for use in novel therapeutics to improve plasma lipid profiles. Specifically, open research questions include how protein inhibitors bind to LPL, how they affect its oligomeric state, and if they cooperate to ensure appropriate physiological regulation of LPL's activity. Another major deficiency in the field is a lack of structural information about LPL. Resolution of an LPL structure would answer the outstanding question of why LPL must be dimeric for activity, and provide a platform for designing therapies aimed at stabilizing endogenous LPL or making stable LPL for enzyme replacement therapy.

A major challenge to using traditional biophysical methods to study LPL structure and function is that LPL undergoes extensive post-translational modification. LPL is both glycosylated and has ten cysteines that form five disulfide bonds. In addition, LPL requires interaction with LMF1, which assists in LPL folding within the endoplasmic reticulum(7,26). These requirements limit LPL expression to mammalian systems. Unfortunately, the purification from mammalian cell culture results in low yields, yet it is the only way to study relevant LPL mutations. Additionally, achieving the high protein concentrations of bovine or human LPL needed for structural biology, analytical ultracentrifugation, and isothermal titration calorimetry is challenging, limiting the use of these technique to understand LPL structure-function relationships and LPL's interaction with regulatory factors. New methods to address these questions and to provide a deeper understanding of LPL's function and structure would improve approaches to target LPL with therapeutics.

Single-molecule techniques provide a novel approach to characterizing LPL by exponentially reducing the quantity of LPL necessary to conduct biophysical measurements. For example, SPR, which has been extensively used by another group to study LPL interactions(99,100), requires several hundred-fold more protein per sample than single molecule experiments. We previously used atomic force microscopy (AFM) to show LPL and ANGPTL4 binding in a defined complex(53), but AFM only provides a snapshot of binding and it cannot provide information on dynamics. I thus turned to single molecule total-internal reflection fluorescence (smTIRF) microscopy as an alternative approach for measuring LPL/partner binding and dynamics as well as LPL structure.

Using smTIRF microscopy, single proteins labeled with a fluorophore can be visualized on the surface of a quartz slide(101). smTIRF provides insights into protein interactions that cannot be derived from bulk measurements, which provide ensemble averages. smTIRF is a well-established technique for studying the dynamics of individual protein-DNA interactions(102-105) and protein-protein interactions(102). Using smTIRF, real-time measurements of dynamics, occurring in individual proteins in response to binding interactions(106), have been observed. smTIRF is also particularly useful to identify and measure the lifetimes of different complexes and transition states(103), as well as conformational changes(107,108). Here, I demonstrate that this technique can be used to study LPL structure-function relationships.

I used fluorescence resonance energy transfer (FRET) to evaluate protein-protein interactions. In FRET, a donor fluorophore is excited by a single laser. When the excited donor fluorophore is close enough to the acceptor fluorophore, non-radiative energy transfer occurs and the acceptor fluorophore releases lower-energy light(109). The energy transfer (E) is dependent on the interfluorophore distance (r) and Förster radius (R_0), a spectral property of the dyes (See Equation 1). Energy transfer therefore can provide an estimate of the distance between the fluorophores. The environment of a dye can influence its R_0.

Equation 1:

$$E = \frac{1}{1+(\frac{r}{R_o})^6}$$

The energy exchange that occurs between dyes also provides an internal control that proteins are localized together. FRET measurements can generate

experimental constraints to support computational models of protein structures or monitor protein dynamics(110-112).

In contrast to FRET, colocalization experiments take advantage of tracking multiple fluorophores by exciting each fluorophore with a laser and identifying spots in which two or more fluorophores are located(113,114). Colocalization is attractive for monitoring the binding of fluorescently labeled substrate or an interacting partner to a labeled LPL dimer. From such experiments, the stoichiometry and dynamics of LPL's interaction with its regulatory factors can be solved. In colocalization experiments the accuracy of measuring complex binding is limited to approximately 300 nm^2(115). Due to non-specific binding to the slide, internal controls for colocalization experiments are extremely important.

The application of these two single molecule fluorescence approaches to study LPL has great potential to impact the field of LPL biology. Without single molecule techniques, LPL studies will continue to be limited by protein concentration and yield. A major obstacle for conducting single-molecule fluorescence experiments is developing the conditions for protein labeling and attachment to slides without affecting the activity of the protein(101). I established methods to begin characterizing LPL interactions and dynamics using these techniques and apply them to outstanding questions in the field. Methods of data collection and analysis are discussed elsewhere(116-119).

Materials and Methods

Molecular Cloning

LPL variants were cloned into pCDNA5/FRT/IRES (ThermoFisher Scientific) with the addition of either a 6x polyhistidine-tag or a V5 tag (GKPIPNPLLGLDST) on the c-terminus. Lmf1 was included in the plasmid to improve LPL folding and secretion. Single cysteines at positions S12, S36, S63, S97, S193, V224, S240, S251, S259, S323, S346, and S384 were introduced using Quickchange site directed mutagenesis. A single cysteine-containing variant of ANGPTL4 was generated by making C76A, C80A mutations in pET16B_ANGPTL4(53). Next, residue A160 of ANGPTL4 was mutated to a cysteine, to provide site-specific modification by a fluorophore.

LPL Protein Expression and Purification

LPL was transiently or stably transfected into HEK 293 FRT Flip-In cells (ThermoFisher Scientific) using Fugene 6. Expression and purification of LPL was carried out as previously described(120). Washing with ≥ 75 column volumes was necessary to eliminate cleavage products. Protein was concentrated, aliquoted, flash frozen in liquid nitrogen, and stored at -80 °C until use or immediately labeled.

Preparation of Fluorescent Cysteine Labeled LPL

Single cysteine mutants of LPL were purified and incubated with an approximately ten-fold molar excess of Alexa Fluor® Maleimide Dyes (Invitrogen). Label was added dropwise to the protein solution followed by gentle mixing. The reaction was allowed to continue, in light protected tubes, for 45 minutes at 4 °C or on

ice. LPL was then diluted 70% with 20 mM Bis-Tris pH 6.5 and re-purified over a HiTrap Heparin Sepharose High Performance Column (GE Healthcare Life Sciences) to remove excess label. Excess label flowed through the heparin column whereas purified, labeled LPL bound and eluted normally. Alternatively, the label could be removed by use of two tandem 7 kDa Zebra desalting columns (ThermoFisher Scientific). LPL samples were aliquoted and stored at -80 °C until use. Samples purified from spin columns were syringe filtered through a 0.2 µm PDVF filter to remove aggregates.

Preparation of Active-Site Fluorescent Labeled and Biotinylated LPL

To label LPL's active site, LPL was incubated for 30 minutes, on ice, with ActivX TAMRA-FP Serine Hydrolase Probe (ThermoFisher Scientific). Next, a 1-2 molar excess of Biotin-N-Hydroxysuccinimide ester (Sigma) was added and the reaction was allowed to proceed on ice for another 10 minutes. LPL was re-purified over a HiTrap Heparin Sepharose High Performance Column (GE Healthcare Life Sciences) to remove excess probe and biotin. Protein could also be desalted using two tandem 7 kDa Zebra desalting columns (ThermoFisher Scientific). LPL samples were aliquoted and stored at -80 °C until use.

Activity of LPL on a Surface

A 96-well black-sided, clear-bottom plate was functionalized by brief incubation with biotinylated bovine serum albumin (Sigma, 1 mg/ml, 5 minutes), three washes with PBS, incubation with streptavidin (Invitrogen, 0.1 mg/ml, 20 minutes) and washing

with PBS. The plates sat on ice with PBS in the wells until the experiment was ready to proceed. Wells were then treated as follows: A) No LPL (Buffer), B) biotinylated bovine LPL (~150 nM, 5 minute incubation), C) Heparin-Biotin (Sigma, 1 mg/ml, 5 minutes) + bovine LPL (150 nM, 5 minutes). Wells were washed three more times with PBS and substrate was added (150 mM NaCl, 0.4% Triton-X, 20 mM Tris 8.0, 14 µM DGGR). Wells were excited at 529 nm with a 590 nm cut-off and read for emission at 600 nm on a SpectaMax 5 plate reader.

Activity of Fluorescently Labeled LPL

Purified LPL^{S384C} was modified as described above with Alexa Fluor®647 dye and desalted through a 7 kDa Zebra desalting column (ThermoFisher Scientific). The protein was then quantified. The activity of equal concentrations of labeled and unlabeled LPL^{S384C} was measured as previously described[53], with the addition of 1 mM deoxycholate.

Single Molecule TIRF Microscopy Slide Preparation

Home-built flow cells on quartz slides were prepared as previously described[119]. The surface of the slides was pre-functionalized by brief incubation with biotinylated bovine serum albumin (Sigma, 1 mg/ml, 5 minutes), washing, and followed by incubating with streptavidin (Invitrogen, 0.1 mg/ml, 20 minutes) and washing. For slides utilizing heparin attachment, biotin-heparin (Sigma, 1 mg/ml, 5-10 minutes) was also added directly to the slides. Immediately preceding data collection, LPL or biotinylated LPL was deposited onto the slide surface and allowed to bind for

approximately 5 minutes. Experiments were carried out in Buffer A (50 mM Tris, 100 mM sodium acetate, pH 7.8).

Unbound LPL was then washed out with Buffer A. Imaging buffer was then added to the slides (Imaging Buffer = Buffer A plus an oxygen scavenging system (2% glucose (Sigma), 1% β-mercaptoethanol (Sigma), 0.1 mg/mL glucose oxidase (Sigma), and 0.025 mg/mL catalase (Sigma)) to prolong the fluorophore lifetime and a triplet state quencher (~50 µM cyclooctatetraene (Sigma)) to lessen fluorophore blinking.)

TIRF Microscopy Imaging

The slides were imaged using a through-prism TIRF laser microscope. Fluorophore excitation was achieved using constant illumination with 532 nm and 638 nm lasers. The fluorophore emissions were collected through a 60X water immersion 1.2 N.A. objective, and the image was split using a DualView optical splitter (Chroma) equipped with a 645 nm dichroic mirror. The emission signals passed through optical filters before detection with a Cascade 512 (Photometrics) emCCD camera: a 585/70 bandpass filter (Chroma) for the TAMRA/Alexa Fluor®555 emissions and a 655 nm longpass filter (Chroma) for the Alexa Fluor®647 emissions were used. Movies of approximately 110 seconds in length were collected at a 100 ms frame rate, using software written in house.

LPL-LPL Interactions Visualized by TIRF Microscopy

Experiments were carried out as described above using the biotin-heparin mode of attachment, and a "Buffer A" containing 50 mM Tris, 300 mM sodium chloride, 5 % glycerol, 1 mM deoxycholate, pH 7.5. LPL molecules were fluorescently labeled, as described above, at specific cysteine residues and mixed together immediately preceding imaging. Residual LPL was then washed off the slides. For the experiments shown, buffer with only cyclooctatetraene or no oxygen scavengers was used to promote fluorophore bleaching. During image capture, only the red (acceptor) laser was turned on for the first 10 frames and again after the 1000th frame. From frames 10-1000, only the green laser was turned on to visualize FRET.

Single Molecule TIRF Data Analysis

The fluorescence intensities of single molecules were extracted from the movies using in house software, as previously described(121). Traces were analyzed only if LPL fluorescence intensity was present at the start of the movie. Time traces with intensities above or below threshold intensities (empirically determined) for single molecules were excluded from further analysis. The remaining intensity traces were then smoothed using a non-linear Chung-Kennedy filter that preserves edges(122,123).

LPL-LPL interactions were analyzed and the average FRET values of the bound complex were calculated. ANGPTL4 binding events were observed as brief periods of Alexa Fluor®647 emission. Two automated methods to detected changes in fluorescence intensity were used: i) a Gaussian kernel method described

previously(103), and ii) a method using the point-by-point standard deviations from the Chung-Kennedy filter. For ANGPTL4 binding to LPL, the transitions were then used to calculate dwell times of the binding events. Hundreds of dwell times were collected, and KaleidaGraph was used to fit each data set to the equation for single-exponential decay ($y = y_0 * e^{-kt}$). To compare dwell times from different protein variants, a half-time for each variant was calculated ($t_{1/2} = -\ln(1/2)/k$). Standard error is reported.

Part 1: Developing Methods LPL for Single Molecule Fluorescence

Attachment of Active LPL to Slides for Single Molecule Fluorescence Studies

Single molecule TIRF microscopy allows for the visualization of single molecules within ~200 nm of the surface of the slide. To monitor a molecule over time, it is necessary to attach the complex to the surface. There are various methods for attaching macromolecules to slides, such as protein-specific binding reagents, antibodies, liposomes, and biotin linkages. The former methods could all be applied to LPL studies, except for liposomes. Liposomes circumvent the need to use protein linkages to attach proteins to slides, but would not be strategic to use with an active lipase. Attaching molecules to slides ensures that they can be monitored over the course of an experiment. Further, using affinity methods for attachment has the advantage that it can help position molecules in the same orientation, with respect to the slide, and provides control over protein deposition.

I devised two approaches, using biotinylated bovine serum albumin (BSA) bound to streptavidin, to attach LPL to slides. BSA blocks nonspecific binding of target proteins and the biotin-strepavidin provides a means to orient biotinylated proteins or

49

conjugates on the surface of the slides. In one approach, I took advantage of LPL's strong affinity for heparin, and utilized biotin-conjugated heparin to bridge LPL to functionalized slides (Figure 3.1A, right panel). Heparin binds to LPL's C-terminus, and has been shown to stabilize LPL against inactivation(124). BSA conjugated directly to heparin is available, but is more expensive than the strategy that I used. In the second approach, I used LPL that was directly biotinylated and then allowed to bind to a BSA-biotin-strepavidin functionalized slide (Figure 3.1A, left panel). Biotinylation of LPL provides a method that may be particularly useful for monitoring LPL interactions that utilize LPL's heparin binding site.

I showed that both biotinylated LPL and the heparin-biotin conjugate were suitable methods for attaching active LPL to slides (Figure 3.1B); however, because the biotin ester can covalently react with any available amine, I found that excessive biotinylation of LPL reduces its activity, thus using a very small molar excess of biotin to modify LPL, along with a short incubation period, is necessary to maintain low-labelled, active protein, as shown (Figure 3.1B). The heparin-biotin conjugation does not have this undesirable effect. In fact, heparin is known to stabilize LPL and represents a more physiological mode of attachment(124). Accordingly, I used the heparin method for monitoring LPL-LPL interactions and the biotin approach when monitoring binding interactions that may require LPL's heparin binding site. Notably, both methods can be used with LPL purified from milk, plasma, or tissue culture.

Two Methods for Specific Labeling of LPL with Fluorophores

After establishing methods to attach LPL to slides, I determined methods for attaching fluorophores at different, specific locations on LPL. I used two methods for specifically labeling LPL (Figure 3.2A). In the first method, I used maleimide fluorophores that react with free cysteines. I took advantage of the fact that although LPL contains ten cysteine residues, they are incorporated into five critical disulfide bonds, leaving no native cysteines available for labeling. Therefore, I engineered specific labeling sites by introducing additional cysteines. I added an additional cysteine residue either on the lid that covers the active site or elsewhere on LPL (Figure 3.2A, top cartoon). To add non-lid cysteine residues, I chose to mutate serines to minimize potential structural and functional changes. I mapped LPL's 40 serine residues on a computational model of LPL to identify serine residues in distinct regions (near the lid, C-terminus, N-terminus, see Figure 3.2A, B). All serine to cysteine mutants, except LPL[S251C], are secreted, and several exhibit activities similar to wild-type LPL (Figure 3.2C). As expected, LPL with an introduced cysteine are readily labeled with the maleimide dye Alexa Fluor®647, whereas wild-type LPL is not labeled under the same conditions (Figure 3.2D, top panel). In addition, I show that maleimide labeling does not hinder the activity of one of the purified cysteine mutants, LPL[S384C] (Figure 3.2E).

Another method that can be used to label LPL is an activity-based protein profiling (ABPP) probe, ActivX™ TAMRA-FP serine hydrolase probe, which readily labels LPL's active site (Figure 3.2A, bottom image). This labeling method is well suited for studies in which catalytic activity is not essential for interpretation of the data,

such as studies that measure protein-protein interactions. A huge advantage of using ABPP is that it is possible to label active LPL from any source. The commercially available serine hydrolase probe is conjugated to a TAMRA fluorophore, which is compatible with our single molecule approach. Unfortunately, this probe does bind to serum in media, and thus purified LPL should be used. Purified LPL labeled with the serine hydrolase probe is shown in Figure 3.2D, middle panel. A Western blot against LPL, showing total LPL protein, reveals a similar amount of active LPL between the two samples (Figure 3.2D, bottom blot). Finally, because fluorophores are prone to bleaching, I confirmed that LPL remains active in buffers containing oxygen scavengers (Figure 3.3).

Site-specific labeling is particularly important for FRET studies because FRET requires the donor and acceptor dyes to be sufficiently close together and FRET distance measurements depend on the specific locations. It has been previously shown that LPL is a homodimer in which the subunits undergo rapid exchange(21). To measure FRET within the LPL dimer, this rapid exchange allows for two different specifically labeled LPL dimers to be mixed to form LPL dimers containing both fluorophores. To use FRET to measure the interaction of LPL with itself or other proteins, LPL can be labeled with one fluorophore and mixed with a differently labeled LPL or LPL-interacting factor.

Part 2: Visualization of LPL Interactions Using TIRF

Visualizing LPL-ANGPTL4 Interactions Using Colocalization Experiments

Colocalization experiments are particularly powerful for measuring complexes with multiple molecules or proteins (113,114,125). To identify colocalized proteins, both lasers are turned on and the proteins are simultaneously monitored over time for overlap in one spot. The Neher and Erie Labs previously used AFM to show the stoichiometry of LPL:ANGPTL4 binding(53). AFM is unable to provide information on protein dynamics. I thus used colocalization experiments to analyze ANGPTL4 binding to human LPL. In these assays, LPL's active site was labeled using the ActivX™ TAMRA-FP, and then labeled LPL was treated with biotin to facilitate its attachment to a quartz slides for imaging. To label ANGPTL4, I generated an ANGPTL4 variant with a single cysteine at position 160 (see methods). This variant was labeled with maleimide-conjugated Alexa Fluor®647, and the fluorophore-labeled variant was still able to inhibit LPL (Figure 3.4). In these experiments (Figure 3.5A), biotinylated LPL was immobilized on the slide, ANGPTL4 was manually flowed over the slide, and binding to LPL was observed.

Figure 3.5B shows an example trace of an LPL dimer (light grey trace) comprised of two fluorescently labeled monomers bound to the slide. Inspection of these data shows that the dimer remains bound, as seen by constant fluorescence intensity of ~700, until 70-80 seconds. From 70-80 seconds, one of the two fluorophores on the LPL dimer blinks twice, as seen by two brief 50% decreases in fluorescence intensity. Subsequently, both LPL fluorophores bleach at 80 seconds as revealed by the loss of all fluorescence. In contrast to LPL, no ANGPTL4 fluorescence

(black trace) is seen until ~18 seconds when a brief increase in fluorescence occurs, followed by the return of the signal to zero. This increase in fluorescence is a result of ANGPTL4 binding. From this trace, the length of time ANGPTL4 is bound to LPL (dwell time) is determine from the length of time the ANGPTL4 fluorescence signal is present. The lifetime of ANGPTL4 binding to LPL is determined by plotting a histogram of the dwell times measured from hundreds of similar events (N = 322), as seen in Figure 3.5C, and fitting the data to the equation for single-exponential decay(126). The half-life of ANGPTL4 bound to LPL is 3.7 ± 0.2 seconds. By contrast, non-specific binding of ANGPLT4 to the slide (data not shown) occurs with a half-life of ~1 second.

In addition to monitoring the binding dynamics, this experimental setup can also be used to calculate stoichiometries of binding complexes or visualize events where an inhibitor dissociates the LPL dimer. In this example, ANGPTL4 simply binds to and dissociates from LPL. ANGPTL4 does not promote the dissociation of one of the monomers of LPL in this case because dissociation of a monomer would result in 50% decrease in fluorescence in the LPL trace when ANGPTL4 dissociated. We did observe two LPL blinking events from ~70-80 seconds, in which half of the LPL signal was lost and then quickly returned, but they occurred much later than ANGPTL4 binding. We then observed an LPL bleaching or dissociation event, in which all of the LPL signal was lost at ~80 seconds. Together, the distinct and equal blinking and bleaching events seen in Figure 3.5C, suggest that in this trace LPL is in a dimeric complex.

Use of Intermolecular FRET to Measure LPL Dimer Dynamics and Structure

Another approach to monitoring protein interactions is FRET. FRET values can be used to estimate the distances between dyes (116,117). Each FRET fluorophore pair has a given distance, R_0, at which half of the energy is transferred. For the fluorophores used here (Alexa Fluor®555 and 647), the calculated R_0 distance is approximately 51 angstroms. This distance can vary slightly depending on the orientation of the fluorophores and their environment, but use of the same dye pair within a complex allows the measurements to be analyzed relative to one another.

The number of interactions that can be monitored simultaneously via FRET is limited by the number of fluorophores that can be tracked, which is limited by the spectral properties of the fluorophores. Previous reports have used up to four dyes for FRET(102,127-129). We found that LPL is well suited for FRET studies as each monomer can be labeled with a different fluorophore and mixed, resulting in a dimer that undergoes FRET.

To generate distance constraints for a model of LPL's structure, hundreds of individual FRET measurements, for multiple sets of LPL mutants, could be collected and plotted as a population in a histogram. Based on a Gaussian fit, an average FRET value (and distance) for each mutant pair is then calculated. FRET distances from many combinations of LPL cysteine mutants can be used to constrain a computational dimer model. Measuring distances between LPL dimer partners using a single molecule approach has the distinct advantage of allowing selection of only those complexes with one donor and one acceptor for analysis. Notably, if these measurements were done in bulk the FRET values would be artificially low because

populations with no acceptor would give off high donor fluorescence and thus reduce the apparent FRET.

To monitor FRET, an automatic alternating laser system was used to toggle lasers (see methods). Time traces for individual molecules were extracted and analyzed. Traces were then manually sorted and only FRET events that involved one acceptor and one donor, as evidenced by single step changes in intensity to zero from blinking or bleaching events, were analyzed.

Example FRET data are shown in Figure 3.6. An in-depth discussion of the analysis methods can be found in previous literature (106,130). We explain these examples, and apply the experiments towards resolving a more-accurate LPL structural model. In Figure 3.6A, structural depictions for each set of mutants are provided. Panel 1 shows the LPL dimer composed of two monomers where the cysteine mutant is introduced into LPL's lid (LPL^{V224C}). Each subunit of the mutant is labeled with maleimide-conjugated Alexa Fluor®555 (donor, green) or Alexa Fluor®647 (acceptor, red). In the second panel, LPL^{V224C*green} was combined with LPL^{S259C*red}. LPL^{S384C*red} is combined with LPL^{S384C*green} in the third panel and LPL^{S36C*green} in the final panel. Labeled monomers were mixed and attached to slides functionalized using the biotin-heparin method we describe above.

Inspection of the traces shown in Figure 3.6B reveals changes in red and green fluorescence first as the green laser switches on (at approximately 1.5 seconds in all the traces) and then as the donor (green) fluorophore bleaches before the end of each trace. The FRET values shown in the lower panel, Figure 3C, were calculated using the formula $I_A/(I_D + I_A)$ where I_D is the donor intensity and I_A is the acceptor intensity.

Throughout the course of the fluorescence traces some small anticorrelated changes can be observed, suggesting small-scale protein movements. Other conformational changes also occur, suggesting the protein changes states. In Figure 3C, panel 1, there is a small but steady decrease in FRET from approximately 4.5 seconds until the donor bleaches. Although it is possible that the donor LPL dissociated and was replaced by a different, unlabeled, molecule, the loss of green fluorescence in panel 1 is most likely a bleach because the intensity goes to zero without many small changes in FRET. In the second panel, which shows LPL^{V224C*green} combined with LPL^{S259C*red}, several small changes in FRET can be observed before the acceptor vanishes, suggesting a conformational change as the acceptor labelled monomer leaves. Shortly after the LPL^{S259C*red} leaves, the donor also bleaches.

The fluorescence and FRET for panel 3 is rather unremarkable, but panel 4 is much more interesting. In panel 4, LPL^{S384C*red} and LPL^{S36C*green} are on the surface and start at a high FRET state near 1.0. At approximately 3 seconds, a conformational change occurs that results in a rapid decrease, but not loss, in the FRET. From there, an additional conformational change occurs in which the FRET slightly increases, at approximately 6.5 seconds.

Data for hundreds of molecules undergoing FRET was analyzed and individual protein states were identified. For each state, a representative sample of 10 FRET points was taken, pooled with the rest of the data for that mutant, appropriately binned, and plotted in a histogram representing the entire population (Figure 3.6D, all panels). A Gaussian curve was used to fit the populations of each histogram and calculate a

mean FRET value(s). These values were then converted into distance measurements using Equation 1 from earlier in this chapter.

In Figure 3D, panel 1, the FRET efficiency from one LPL^{V224C} to the next was found to be 0.62 which is an estimated distance of 47 angstroms. In our final histogram, the two states seen in the trace are not obvious, probably because they are quite popular and near the R$_0$, which is the most sensitive region.

As shown in panel 2, the histogram for LPL^{V224C} to LPL^{S259C} reveals one major population at 0.81, with secondary states around 0.43 and 0.67. These distances correspond to 40, 45, and 53 angstroms, respectively. Likewise, the histograms for FRET efficiency between LPL^{S384C} and LPL^{S384C} or LPL^{S36C} show one major and one minor peak, indicating that at least one labelled mutant position adopts two conformational states. The populations had FRET values of 0.43 and 0.88 for the mutant with itself and 0.52 and 0.82 for LPL^{S384C} with LPL^{S36C}. These values correspond to estimated distances of 53, 37, 50, and 40. These similar populations suggest that the dimers may be approximately halfway offset to one another. We used distances derived from the most prevalent state for modeling.

Initial Modeling of LPL Dimers

Although structural models of LPL exist, current models are only computationally derived(131). In particular, little is known about the LPL dimer orientation and no true structural models of the dimer exist. Adding FRET-generated distance constraints would enhance structural models. Studies support the homodimer being in a head-to-tail conformation(9,24), but how the dimers are

docked remains a mystery. Mike Lafferty in the lab undertook studies of LPL

modeling. First, he used HADDOCK (132) to dock the LPL dimer. The results of the

docking suggested three possible head-to-tail conformations (Figure 3.7). Figure

3.7A shows a model in which the lids are buried next to each other within the dimer

interface. Figure 3.7B is where the lids are still next to one another, but less buried in

the interface. The model in Figure 3.7C positions the lids near the lipoprotein binding

site on the opposite protein's C-terminus.

This final model makes the most scientific sense in that the lids likely would

not clash when they open. Based on previous studies aimed at modeling LPL, it is

known that the active sites use the opposite dimer's lipoprotein binding region, on

the C-terminus, for long-chain substrate binding. When the three tryptophan

residues, responsible for long chain substrate binding are mutated, the opposite LPL

molecule can only hydrolyze short chain substrates (24).

When we looked at the FRET derived distances and compare them to the

predicted distances from the HADDOCK models, the experimental data did not

support the models. For the third model, the modeled distances were 34 angstroms

for the LPL^{V224C} positions, 25 angstroms for the LPL^{V224C} LPL^{S259C}, 34 for LPL^{S384C} to

itself and 42 angstroms for LPL^{S384C} to LPL^{S36C}. This model, with the mutations

labelled, is shown in Figure 3.8. These distances are shorter than the experimentally

determined distances, suggesting the need for better models.

Rosetta Was Used to Generate Refined Models

Mike used Rosetta to produce more refined dimer models. Mike input an LPL monomer and let Rosetta dock the dimer into the most energetically favorable positions using either rigid or global docking. In rigid docking, the individual monomer backbones are kept rigid, but whole-monomer and sides chain movements are allowed while in global docking, the monomers can undergo larger conformational changes to adjust to a more energetically favorable position.

Several of the best resulting models are shown in Figure 3.9 A-F. Models A and B are renditions of the third HADDOCK model, but the dimer is much more condensed and the dimers less offset. Models A and B both had distances closer the experimental data, except for the pair LPL^{S384C} and LPL^{S36C}, which had a shorter predicted distance than my data suggests. A model somewhere between the third HADDOCK model and these models would likely be the best fit for a head-to-tail confirmation.

Models C and D have the lids quite near one another, instead of near the substrate binding site. Using the distances generated from Figure 3.6, I eliminated models C and D, which had LPL^{V224C} - LPL^{V224C} measurements of 30 and 10 angstroms, respectively, which does not fit the experimental data well. Finally, Models E and F were odd models that had mostly favorable distances, but they do not fit the expected head-to-tail conformation despite their distances being a good fit for the data. While these models seem an unlikely fit, it's possible that a model that blends models A, B, E, F and the third HADDOCK would be a best fit.

Conclusions and Future Applications of This Method

Here, I describe a single molecule method for measuring LPL interactions through the use of suitable cysteine mutants, labeling strategies, and modes of attaching LPL to slides. I show that fluorophore colocalization is an effective tool to measure the binding of fluorescently labeled LPL regulatory factors, such as ANGPTL4 at a level of detail that cannot be observed through bulk methods. Further, this technique proved effective at monitoring LPL-LPL interactions. Based on the models generated using HADDOCK and Rossetta, two similar models were generated, each with slight variation from the experimental data. To resolve this issue, future studies modelling these structures with the addition of dyes will be conducted to evaluate the best structural model.

In the future, this method will be harnessed to monitor the binding of additional LPL regulatory factors to LPL and monitor changes in LPL's conformation upon binding of a lipid substrate. This is important because how LPL accesses the triglyceride rich core of lipoproteins remains an outstanding question in the field.
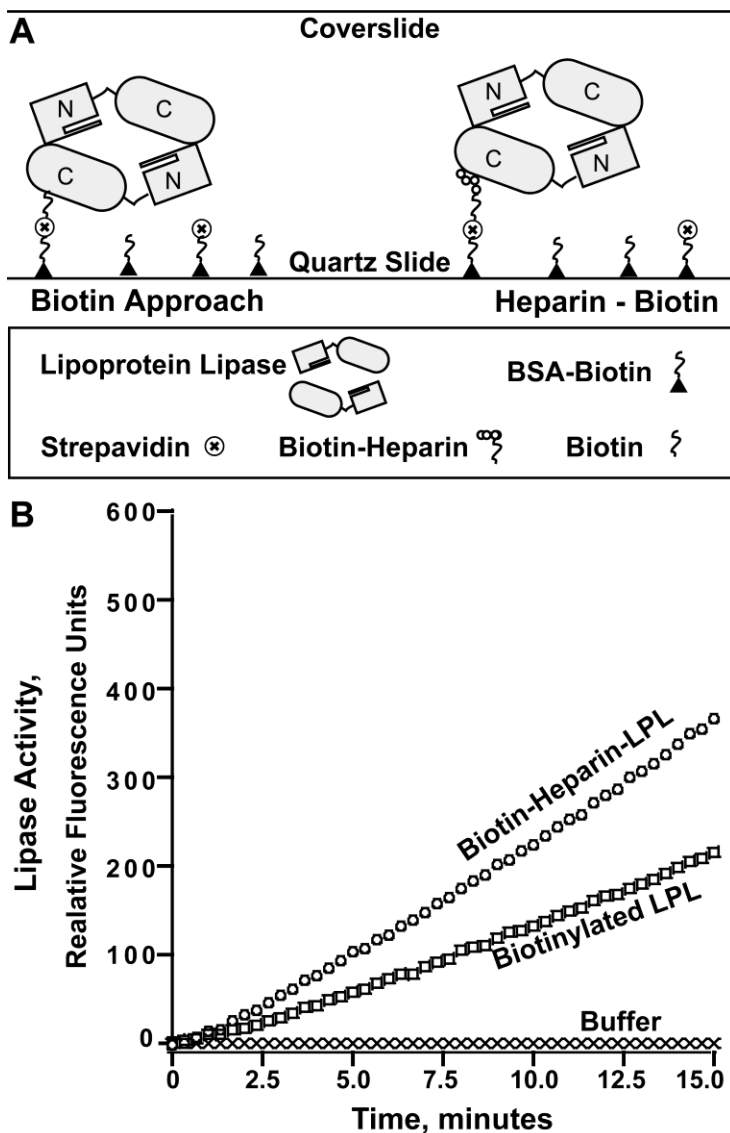
Figure 3.1. Active LPL Can be Attached to a Slide Using Two Methods.
A) Quartz slides can be functionalized for LPL attachment with BSA-biotin, streptavidin. LPL is then attached either after being conjugated to biotin (left) or after the addition of biotinylated heparin (133) to the slide. LPL avidly binds to heparin.
B) LPL remains active on a functionalized surface. LPL was bound to a BSA-biotin-streptavidin coated 96-well plate. The activity of the LPL remaining in the wells after washing was read after the addition of a substrate mixture containing DGGR. Both biotinylated LPL and LPL bound to the surface after functionalization with heparin-biotin were active.
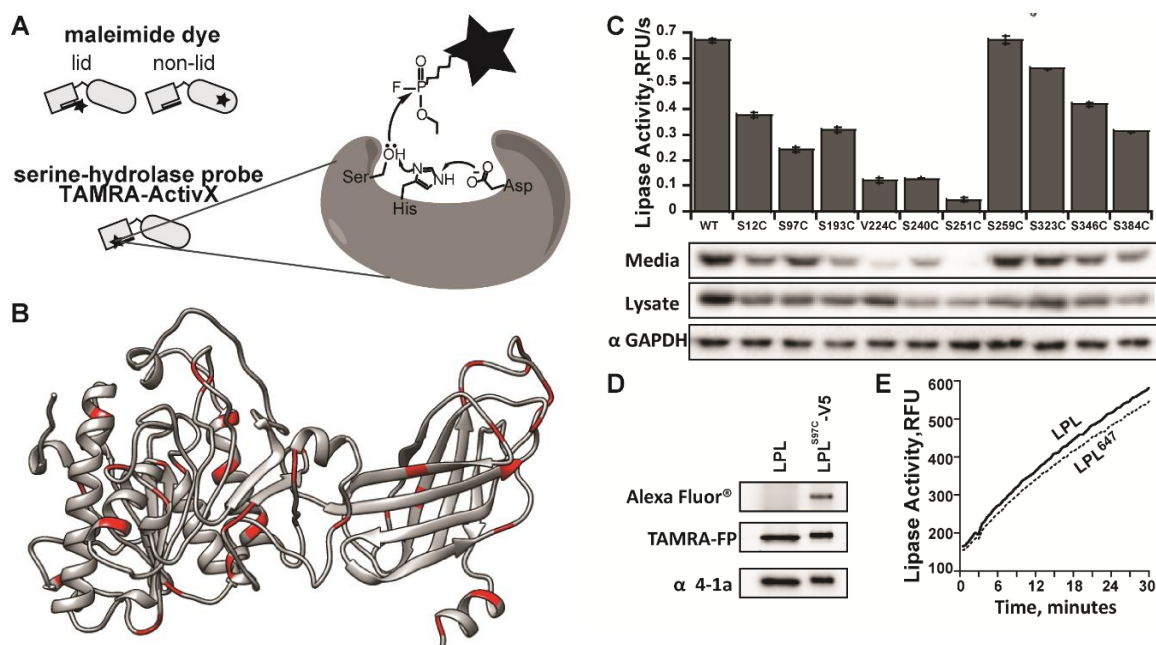
Figure 3.2. Strategies for Fluorescently Labeling LPL.
A) LPL can be labeled specifically using maleimide dyes or covalently in the active site using a serine-hydrolase probe.
B) Serine residues on LPL are labeled in red, on a previously described LPL model(60).
C) LPL cysteine mutants with a V5 tag were transiently expressed and the media was tested for activity, representative data is shown. Secreted (media) and lysate fractions are shown, probed against the V5-tag. A GAPDH loading control for the lysate is shown. The standard deviation of triplicate wells is shown.
D) Wildtype LPL or an LPL^{S97C} with a V5 tag, were labeled concurrently with Alexa Fluor®647 and ActivX-Serine-Hydrolase and then run on a gel and visualized for fluorescence. A western blot against LPL (third panel, α 4-1a) shows total protein.
E) LPL^{S384C} retains activity when labeled with Alexa Fluor®647 maleimide dye (dashed versus solid line).
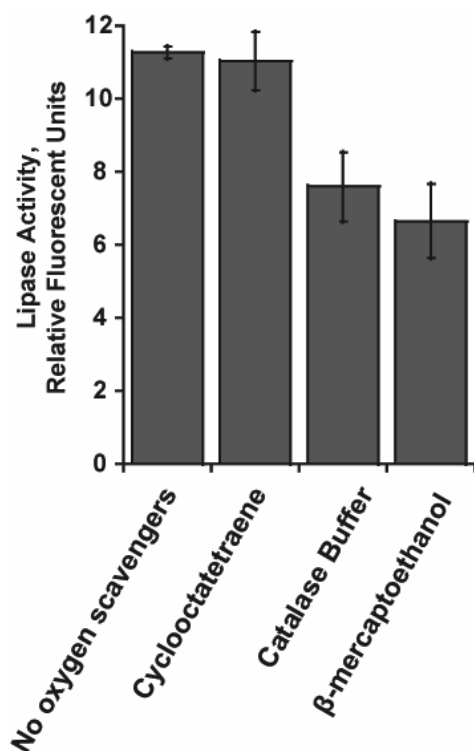
Figure 3.3. LPL Maintains Activity in Oxygen Scavenging Buffers.
5 nM LPL was assayed for activity in the different oxygen scavenging buffers used for imaging, cyclooctatetraene (50 µM), catalase buffer (2% glucose, 1% β-mercaptoethanol, 0.1 mg/mL glucose oxidase, 0.025 mg/mL catalase, and 50 µM cyclooctatetraene), or β-mercaptoethanol (1%). The fluorescent substrate EnzChek (10 µM) was used as previously reported(134) as reducing agents disrupt DGGR measurement. Some loss of LPL activity was seen for buffers containing βME (catalase buffer and βME), but it could be due to disruption of the assay substrate as was seen for DGGR.
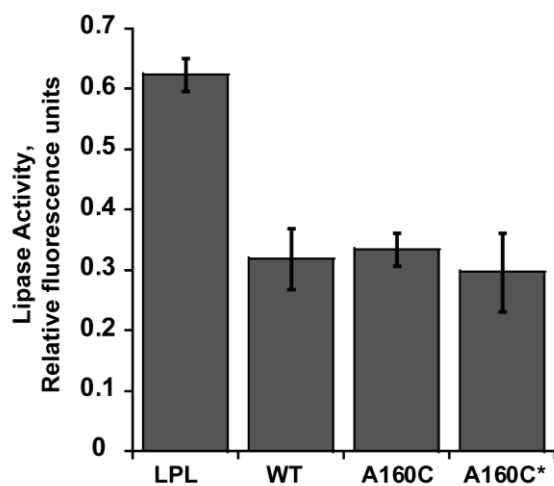
Figure 3.4. ANGPTL4 Labelled with a Fluorophore Can Still Inhibit LPL.
LPL (5 nM) was assayed using DGGR in the absence or presence of an equal amount of wildtype, mutant, or labelled mutant ANGPTL4. Both labelled and unlabeled mutant ANGPTL4 were equally potent LPL inhibitors, compared with wildtype ANGPTL4.
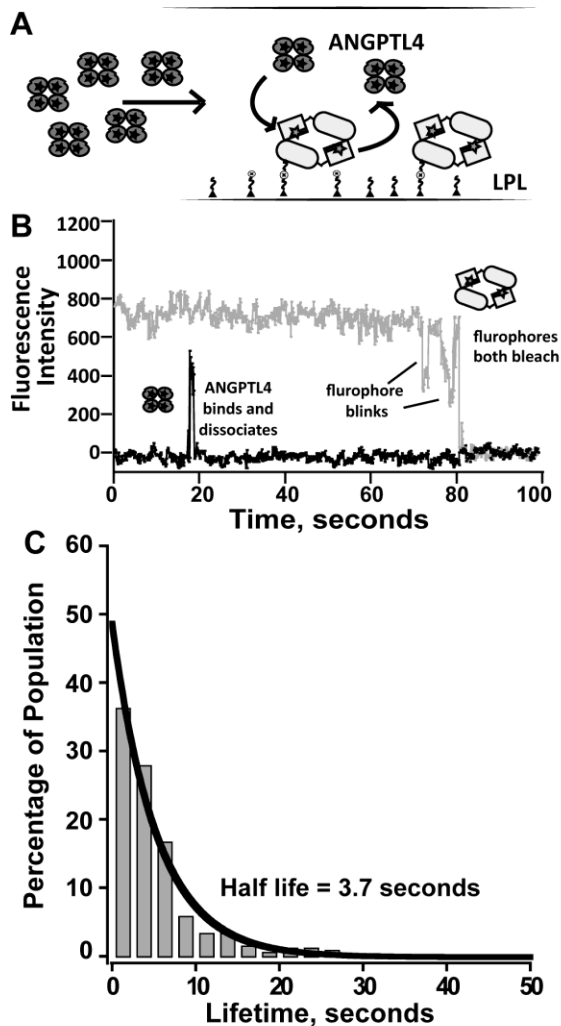
Figure 3.5: Single Molecule Binding of ANGPTL4 to LPL.
A) Labeled LPL is attached to a slide for TIRF imaging. Labeled ANGPTL4 is flowed into the slide, and ANGPTL4-LPL interactions are measured.
B) An example trace showing ANGPTL4 (black trace) binding to LPL (light grey trace).
C) Distribution of the dwell times of ANGPTL4 binding to LPL (N = 322) was fit to the equation for single-exponential decay, then the half-life of ANGPTL4 bound to LPL was determined to be 3.7 ± 0.2 seconds.
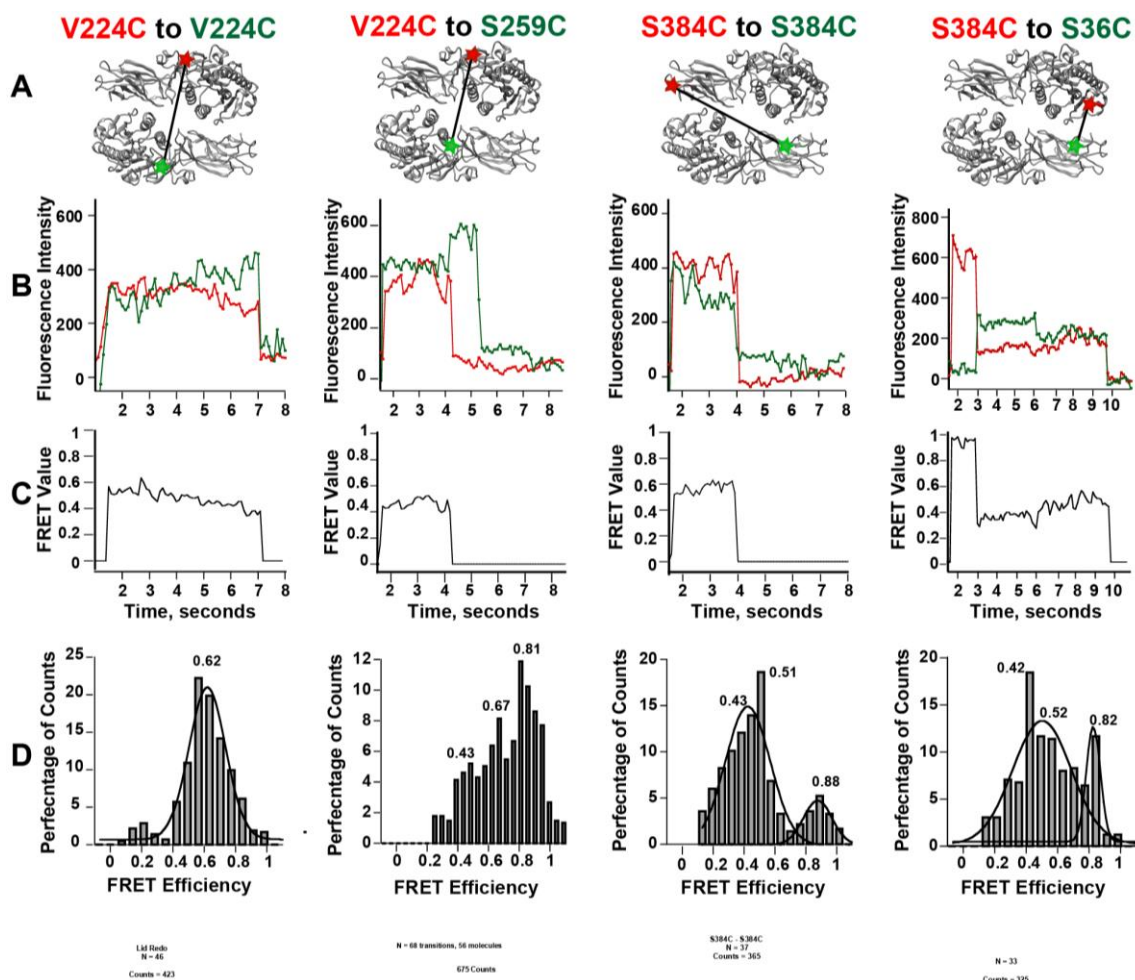
Figure 3.6. Examples of LPL-LPL Intermolecular FRET.
A) Cartoons of LPL dimer mutants, labelled with their respective fluorophores. Green stars represent a donor labelled partner while red represents the acceptor fluorophore attached to the appropriate LPL mutant. The black bar connects the two, showing a relative distance.
B) Example time traces showing dimers bound to the surface and undergoing FRET. As the green laser automatically turns on, fluorescence is observed just before the 2 second mark in each trace. In each case, the green fluorophore vanishes before the end of the trace, marking the donor bleach. In the second panel, the acceptor bleaches first.
C) FRET traces for the fluorescence traces shown in part B are given. In all four panels, the FRET returns to zero when a fluorophore bleaches.
D) Extracted FRET values were plotted as histogram distributions for each mutant. For V224C-V224C, traces from 46 molecules were analyzed. A major population of the FRET efficiency of V224C-V224C is found around 0.62. Traces from 56 molecules, were plotted for V224C-S259C. For this pair, several states are observed with the largest fraction near 0.81. In the third panel data from 37 traces of S384C-S384C were plotted and the Gaussian fit of the FRET efficiency was 0.42 while many the molecules were binned at 0.51. As with the next panel, there is another population present with high FRET. The final panel shows data from 33 molecules of S384C with S36C. Three distinct states are observed, all of which can be seen in the above FRET trace.
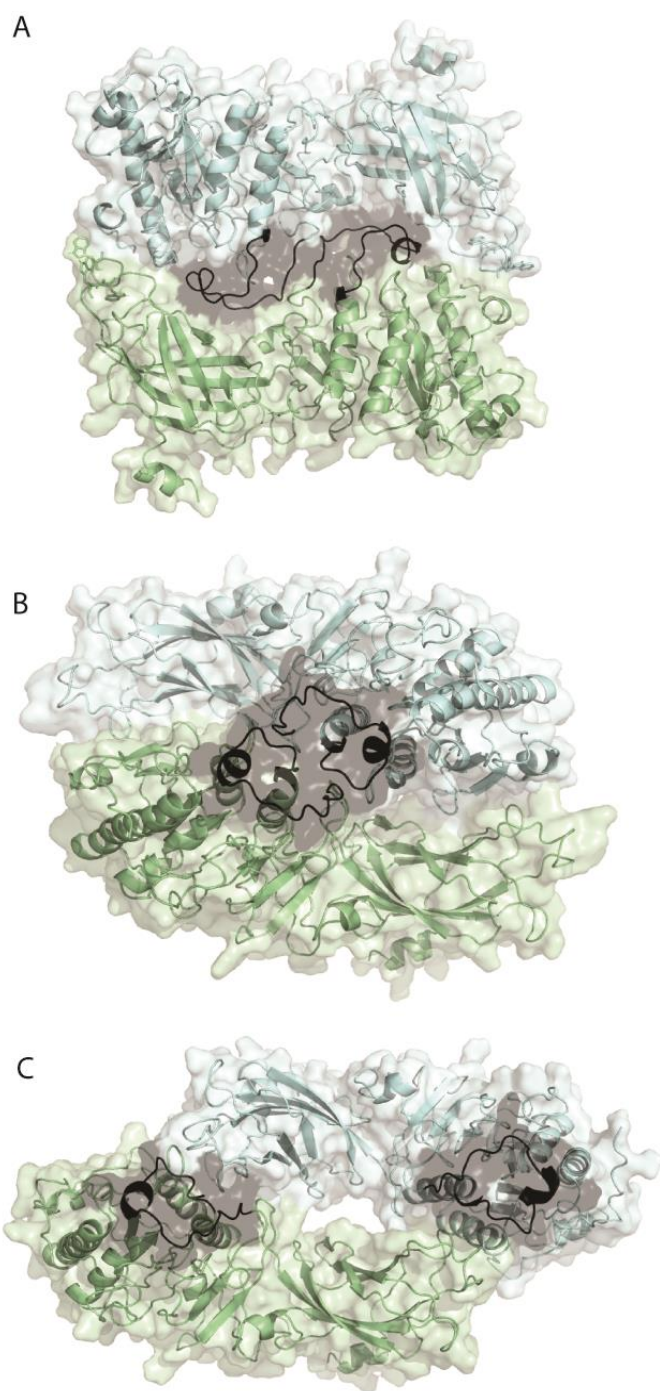
Figure 3.7. LPL Dimer Models Generated by HADDOCK.
The HADDOCK server was used to model docking of LPL as a dimer. Each monomer of LPL is shown as either blue or green, and LPL's lid is shown in black. The three models suggest quite different docking models of LPL in a head-to-tail dimer.
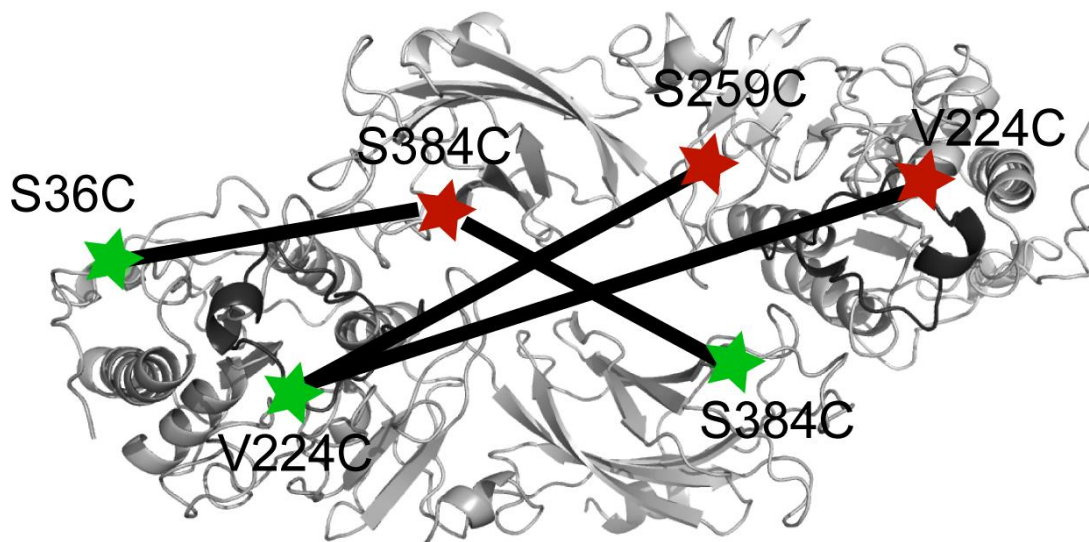
Figure 3.8 LPL Dimer Model Labelled with Appropriate Dye Positions.
The third HADDOCK model from Figure 3.7 is shown here with appropriately labelled
dye positions. While the measured distances were rather short, the relative distances
for the S384C paired donors appears to be consistent with our data. In addition, the
relative distances between V224C and its partners also appears consistent with our
data suggesting this model is reasonable, but more modeling is necessary.
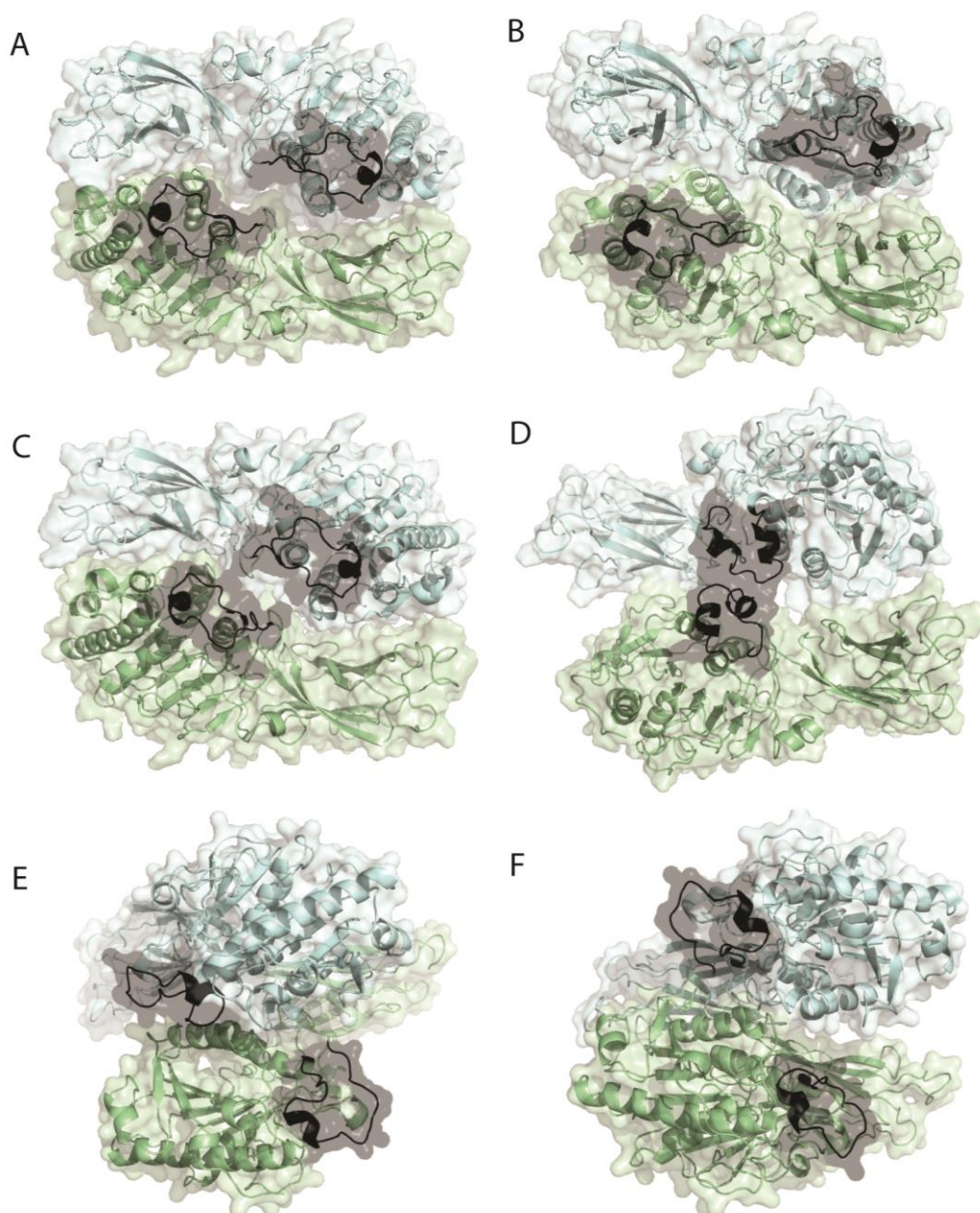
Figure 3.9. A Sample of LPL Dimers Docked Using Rosetta.
Rosetta was used to generated models using rigid body or global docking. A selection of representative models of the top energetically favorable confirmations are shown. Models A and B resemble two dimers with their lids near the lipoprotein/long-chain substrate binding patch. Models C and D show a model where the lids are close to one another and might potentially clash. Models E and F show two models that were generated where the dimers docked in a non-head-to-tail conformation.

CHAPTER 4: CONCLUSIONS AND FUTURE DIRECTIONS

LPL is a critical enzyme in the hydrolysis and breakdown of TRLs. It is the best studied of the three dimeric lipases in its family, yet much remains to be understood about the function of this enzymes and why the three dimeric family members require homodimerization for activity while most human lipases are active as monomers. When I began undertaking the research presented here, few labs readily studied purified human LPL *in vitro*, opting for the more stable, cheaper to purify, bovine LPL or relying on unpurified LPL in tissue culture media, which contains mostly inactive full-length and cleaved protein. Purification of human LPL is a time and resource intensive undertaking, but I have shown here the importance of using the purified enzyme to accurately measure LPL function.

The work presented here highlights my published and ongoing studies to 1) provide a better understanding of ways to improve LPL function, 2) develop a method to better study human LPL interactions, and 3) provide an experimentally based LPL structure.

Improvements in Our Understanding of LPL as a Therapeutic Target

LPL^{S447X} Study Suggest Lipoprotein Uptake is More Important Than TRL Hydrolysis in Individuals with Functional LPL.

My finding that LPL^{S447X} promotes lipoprotein uptake better than wildtype is strongly supported by *in vivo* data showing that LPL^{S447X} carriers have improved triglyceride rich particle clearance(84,96,135). It makes sense that clearance of a partially hydrolyzed triglyceride rich particle from circulation would have a stronger impact on triglyceride levels than hydrolysis of more triglycerides alone as lipoprotein particles contain high concentrations of triglycerides.

Lipoprotein uptake has long been an aim of cholesterol lowering drugs, which often target lipoprotein receptors. For example, studies of individuals with excellent cholesterol levels found that carrying a loss-of-function mutation in proprotein convertase subtilisin/kexin type 9 (PCSK9) was cardio protective(136,137). PCSK9 is a protease that helps target LDLR for lysosomal degradation. Loss of PCSK9 function allows for more LDLR to reach the surface of the liver, thus promoting more LDL uptake and leading to an overall decrease in circulating LDL levels. This recent finding led to a rush for the development of drugs aimed at downregulating PCSK9 in an effort to improve cholesterol levels. Two medications are already available, alirocumab and evolocumab(138,139). Others are rushing to produce more drugs with the same affect using antibodies(140), vaccines(141,142), and *in vivo* gene editing(143). An approach to lowering triglycerides might entail similar approaches.

72

In fact, my lipoprotein uptake hypothesis was prompted by population studies in which it was often found that women, who often have lower triglycerides on average, do not often have the same benefit from carrying the mutation as men(72). Women's lower circulating triglycerides could be due to estrogen's ability to upregulate LDLR production, perhaps through regulation by PCSK9(144). Due to side effects, estrogen therapy would not be a good treatment for hypertriglyceridemia, but the contrasting difference between men and women does highlight how upregulation of lipoprotein uptake receptors are a suitable and reasonable approach to treating people suffering from hypertriglyceridemia.

Another implication of the work I presented above is that lipoprotein uptake alone may be a useful treatment for people with properly functioning LPL, but elevated triglycerides. Patents are already in place for LPL enzyme replacement therapy; however, such therapies will be challenged by the poor yield and stability of human LPL. In contrast to full-length LPL, LPL's C-terminus can be purified from *E.coli* and is capable of promoting lipoprotein uptake(98). While conducting my lipoprotein uptake assays, I used bovine LPL as a positive control and found that I needed 10-20 fold more bovine LPL to promote approximately equal lipoprotein uptake compared to the minimal levels of human LPL necessary. This highlights the importance of using human LPL for enzyme replacement, and it also suggests a possible combination therapy with purified full-length active bovine and human C-terminus.

LPL Regulation by ANGPTL4 and GPIHBP1

There are conflicting reports about how ANGPLT4 and GPIHBP1 compete for LPL binding. My data contributes to resolving this conflict. One group has shown that GPIHBP1 can protect LPL from ANGPTL4 inhibition(57) while another found that ANGPTL4 strips LPL from GPIHBP1 anchors on cells(58). Although these studies differ in that the former used purified proteins *in vitro* and the latter uses cells in culture, my data supports the later work by Brandon Davies' lab that suggests GPIHBP1 does not protect LPL from ANGPTL4 inhibition.

My hypothesis is that ANGPTL4 has two mechanisms that result in LPL inhibition. First, ANGPTL4 briefly binds to LPL during which it inhibits substrate hydrolysis. Second, when ANGPTL4 binds to LPL, it also knocks off stabilizers, such as GPIHBP1 or deoxycholate. This removal of stabilizers leaves LPL *"naked and alone"* and susceptible to heat inactivation after ANGPTL4 dissociation.

Our group previously showed that ANGPTL4 is a reversible LPL inhibitor(53), but controversy remains over the inclusion of deoxycholate, a bile acid, in these assays. In my hands, human and bovine LPL have a similar K_i for ANGPTL4 inhibition, when assayed in the presence of deoxycholate. When I assay low concentrations of human LPL in the absence of stabilizers, like deoxycholate (a naturally occurring bile salt) or GPIHBP1, the LPL rapidly inactivates in the absence of ANGPTL4. In the presence of stabilizers, which likely represents a more physiological situation, LPL is fairly resistant to heat inactivation, but still inactivates in the presence of ANGPTL4. My unpublished data has shown me that bovine LPL is considerably more stable than human LPL. The difference between these proteins

may be best explained by their production. Bovine LPL is purified from cow's milk, which is rich in small molecules potentially capable of stabilizing LPL, while human LPL is purified from low-serum tissue culture media. Further studies will be necessary to identify the small molecule(s) that bind and stabilize LPL milk and plasma.

Single Molecule Experiments Provide a New Avenue for Understanding LPL

While lipoprotein uptake is presumably a starting point for helping individuals suffering from elevated triglyceride rich lipoproteins, my study shows how important *in vitro* biochemistry is in answering fundamental biological challenges. Many of the outstanding questions in the LPL field remain biochemical questions as LPL cannot be assayed using most traditional biophysical measurements. When I turned to a single molecule approach to studying LPL, I welcomed a method that would allow us to see not only how individual LPL molecules responded to different stimuli, but also generate distance constraints for a better LPL model.

ANGPTL4 Binding to LPL is Short-lived.

As emphasized throughout this thesis, LPL is a highly regulated enzyme, yet little is known about how its factors bind and alter LPL's function. We know little about where proteins interact with LPL, their stoichiometry, and how they alter LPL's structure or function. I decided to study an interaction our lab has been intensely interested in, LPL-ANGPTL4. I found that the half life of ANGPLT4 on LPL was fairly short. This fairly transient interaction suggests that the interaction between LPL and

ANGPTL4, at least *in vitro,* is fast enough that a therapeutic against ANGPTL4 might not need to be able to displace ANGPTL4 from LPL, but instead just bind free ANGPTL4 and prevent its rebinding to LPL molecules. A fast interaction time also suggests that if my hypothesis from above about ANGPTL4 leaving LPL *"naked and alone"* is true, then it is equally important to focus therapeutics on stabilizing LPL instead of reducing inhibition of LPL by ANGPTL4.

FRETting Over a Better LPL Dimer Model

A major challenge to understanding LPL and designing therapeutics to stabilize it is the lack of a structural information about LPL. When I set out to develop a single molecule FRET-constrained model, I was hoping to resolve this issue. From the models we generated, there were two major structural orientations for the dimer (see previous chapter) supported by my data. The structural model that is supported by previous studies is one that encompasses elements of models A and B along with the third HADDOCK model. These models appear to be extremes of the best LPL model that fits the head-to-tail conformation. They are broadly similar to each other and to the previously published LPL dimer models, but differ enough to have significantly different distances. Moving towards a better "blended" model in which the long chain substrate binding site is near the active site requires consideration of the populations present for each set of mutants.

When I first evaluated data, I only had data from the LPL^{V224C} combinations, which both strongly supported Rosetta models A and B over the HADDOCK model. Once I added the additional constraints involving the LPL^{S384C} pairs, the data

suggested a divergence from the two Rosetta models. The data shown in Chapter 3

suggests a model in which LPL^{S384C} and LPL^{S36C} on one monomer are

approximately the same distance from LPL^{S384C} on the other, most like the

HADDOCK model. Inspection of the histograms for these later pairs reveal that the

major population of LPL^{S384C} to LPL^{S384C} is skewed towards longer, lower FRET,

distances while the major population for LPL^{S384C} to LPL^{S36C} appears to be skewed

towards shorter. This supports a "middle ground" between Rosetta models A and B

and the third HADDOCK model, with the dimer being slightly more shifted in favor of

S36C being shorter than S384C to itself. With the data from LPL^{V224C} pairs being

longer than the HADDOCK model, it seems likely an outward rotation along the X-

axis for both dimers would be needed to increase the space between the partners, in

addition to the translation along the X-axis to correctly position LPL^{S384C} and LPL^{S36C}.

I am currently working with a collaborator to add dyes into the models and

improve upon the models by constraining them with the dye distances I have

generated. This new model will provide the first truly experimentally supported

structure.

Future Directions for Single Molecule Experiments

In my studies using smTIRF in Chapter 3, I describe methods and

experiments that I devised to address just a few outstanding questions about LPL.

There are many future advancements and tricks that could be used to make this

technique suitable for understanding additional questions. In addition, there are

several outstanding questions about LPL that will greatly benefit from single molecule studies. I briefly discuss these future directions below.

Future Advancements in the Experimental Setup

I provide one suitable method of attachment for LPL to slides, but several other interesting possibilities open the door for more studies. One major advancement would be using biotin-PEG functionalization instead of BSA, to reduce non-specific binding. The Erie Lab has recently adopted this protocol with the availability of a reasonably affordable non-fluorescent PEG stock. This attachment method should be utilized in future studies, especially those aimed at measuring regulatory factor interactions with LPL.

Another way surfaces are often functionalized is by encapsulating protein in biotinylated liposomes. As mentioned in Chapter 3, this is not a good idea for encapsulating an active lipase, however it would be an excellent way to visualize LPL's interaction with fluorescently labelled apolipoproteins added to the surface of the liposomes, representing mimetic lipoproteins. Lipoproteins could also be potentially biotinylated and utilized in the same manner.

LPL – Apolipoprotein Interactions

Using the liposome attachment method mentioned above, the possibility to measure LPLs interaction with lipoproteins is endless. One major advantage with attaching the lipoproteins to the slide is that LPL could be added to the slide in real-time using a flow cell, which would improve data collection as the LPL can be kept

cold and stable longer than if it is attached to the slide, an advancement that will increase the number of active molecules undergoing FRET.

Two of the apolipoproteins that would be particularly interesting to study are the LPL inhibitor APOC-III and LPL activator APOC-II, which both work by unknown mechanisms. One recent paper suggests that APOC-III inhibits LPL through displacement of LPL from the surface of lipoproteins(41). To further investigate this mechanism, fluorescent APOC-III could be bound to biotinylated liposomes on a surface, and then fluorescent LPL flowed over the surface to determine if APOC-III leaves with LPL when it binds. This would be an elegant experiment that would directly show what happens when APOC-III and LPL interact.

Using a similar experimental setup, APOC-II could also be studied. Recent studies have shown a renewed interest in LPL's most abundant activating factor, APOC-II. Little is known about how APOC-II activates LPL, apart from APOC-II supporting substrate turnover(33). One likely mechanism for this is through modulating substrate access by LPL's lid. If and how APOC-II alters LPL's lid movement would be very interesting, especially since small lid dynamics were observed in my study of the lids undergoing FRET in Chapter 3. Adding back fluorescent APOC-II(36,67) to APOC-II-deficient lipoproteins and seeing how this impacts lid movement, if at all, will help support a model for creating the most efficient version of LPL.

Visualizing LPL's Lid Movement

As mentioned above, small transitions were observed when the LPL Lid mutant, LPL^{V224C} was bound to itself. LPL's substrate hydrolysis is mediated, like most lipases, by its lid, but how LPL's lid functions to govern substrate entry remains a mystery. *In vitro* activity assays reveal that LPL can hydrolyze short chain substrates in the absence of a full-length lid, supporting a hypothesis that LPL's lid does not mediate hydrolysis, but instead is more important for substrate specificity. In my data, some transitions showed a decrease in FRET while others showed an increase, suggesting one monomer's lid was moving slightly in the opposite direction of the other with no definite pattern. The movement in LPL's lid may represent LPL sampling available space for suitable substrates. I have a single trace of preliminary data, not included here, in which an LPL dimer undergoes FRET in the presence of TRLs. In this trace, the FRET seems to increase steadily and then sharply drop several times over the course of the trace, perhaps suggesting LPL's lid is opening and closing. Extensive studies will need to be conducted in the future to see if the data I showed can be recapitulated, especially in the presence of fluorescently labelled lipoproteins. If LPL's lid is required to open and close for each cycle of substrate hydrolysis, this suggests that a small molecule aimed at holding LPL's lid open is not a suitable therapeutic.

Single Molecule Studies to Reveal ANGPTL3 and ANGPTL8 Mechanics

Here, I showed that ANGPTL4 binding to LPL occurs over a short lifetime measurable by smTIRF. It is presumable that the other ANGPTL proteins, ANGPTL3

and ANGPTL8, also interact with LPL on a similar timescale. It was recently shown that *in vivo*, you need ANGPTL3 for ANGPTL8 to be active while ANGPTL3 can act independently(49). The structural and oligomeric requirements for this inhibition remain a mystery. While our lab was able to visualize ANGPTL4 tetramers bound to LPL dimers using AFM(53), it would be hard to distinguish ANGPTL3 and ANGPTL8 from each other via AFM. SmTIRF could thus be used to monitor complex binding where the ANGPTLs are labeled with two distinct dyes such that the stoichiometry and binding dynamics could be determined. This detail could not be observed using SPR or other available biochemical techniques.

Conclusions

In conclusion, LPL is a revolving therapeutic target with many angles for pharmaceutical intervention. In this thesis, I highlighted how biochemistry was necessary to explain how a gain-of-function LPL mutant, LPL[S447X] and I provide a new approach to biochemically characterizing LPL, single molecule fluorescence, and use that technique to move towards a better model of the LPL dimer. Single molecule studies, in addition to the new dimer model, will open a wide possibility for different studies imagined here, as well as by others.

REFERENCES

1.   Miller, M., Stone, N. J., Ballantyne, C., Bittner, V., Criqui, M. H., Ginsberg, H. N., Goldberg, A. C., Howard, W. J., Jacobson, M. S., Kris-Etherton, P. M., Lennie, T. A., Levi, M., Mazzone, T., and Pennathur, S. (2011) Triglycerides and cardiovascular disease: a scientific statement from the American Heart Association. *Circulation* **123**, 2292-2333

2.   Beisiegel, U., Weber, W., and Bengtsson-Olivecrona, G. (1991) Lipoprotein lipase enhances the binding of chylomicrons to low density lipoprotein receptor-related protein. *Proceedings of the National Academy of Sciences* **88**, 8342-8346

3.   Krapp, A., Zhang, H., Ginzinger, D., Liu, M. S., Lindberg, A., Olivecrona, G., Hayden, M. R., and Beisiegel, U. (1995) Structural features in lipoprotein lipase necessary for the mediation of lipoprotein uptake into cells. *J Lipid Res* **36**, 2362-2373

4.   Nykjaer, A., Nielsen, M., Lookene, A., Meyer, N., Roigaard, H., Etzerodt, M., Beisiegel, U., Olivecrona, G., and Gliemann, J. (1994) A carboxyl-terminal fragment of lipoprotein lipase binds to the low density lipoprotein receptor-related protein and inhibits lipase-mediated uptake of lipoprotein in cells. *J Biol Chem* **269**, 31747-31755

5.   Williams, S. E., Inoue, I., Tran, H., Fry, G. L., Pladet, M. W., Iverius, P. H., Lalouel, J. M., Chappell, D. A., and Strickland, D. K. (1994) The carboxyl-terminal domain of lipoprotein lipase binds to the low density lipoprotein receptor-related protein/alpha 2-macroglobulin receptor (LRP) and mediates binding of normal very low density lipoproteins to LRP. *J Biol Chem* **269**, 8653-8658

6.   Rodrigues, R., Artieda, M., Tejedor, D., Martinez, A., Konstantinova, P., Petry, H., Meyer, C., Corzo, D., Sundgreen, C., Klor, H. U., Gouni-Berthold, I., Westphal, S., Steinhagen-Thiessen, E., Julius, U., Winkler, K., Stroes, E., Vogt, A., Hardt, P., Prophet, H., Otte, B., Nordestgaard, B. G., Deeb, S. S., and Brunzell, J. D. (2016) Pathogenic classification of LPL gene variants reported to be associated with LPL deficiency. *Journal of clinical lipidology* **10**, 394-409

7.   Doolittle, M. H., Neher, S. B., Ben-Zeev, O., Ling-Liao, J., Gallagher, C. M., Hosseini, M., Yin, F., Wong, H., Walter, P., and Peterfy, M. (2009) Lipase maturation factor LMF1, membrane topology and interaction with lipase proteins in the endoplasmic reticulum. *J Biol Chem* **284**, 33623-33633

8.   Young, S. G., Davies, B. S. J., Voss, C. V., Gin, P., Weinstein, M. M., Tontonoz, P., Reue, K., Bensadoun, A., Fong, L. G., and Beigneux, A. P. (2011) GPIHBP1, an endothelial cell transporter for lipoprotein lipase. *Journal of Lipid Research* **52**, 1869-1884

9.   Wong, H., Yang, D., Hill, J. S., Davis, R. C., Nikazy, J., and Schotz, M. C. (1997) A molecular biology-based approach to resolve the subunit orientation of lipoprotein lipase. *Proc Natl Acad Sci U S A* **94**, 5594-5598

10. Lowe, M. E. (1997) Structure and function of pancreatic lipase and colipase. *Annu Rev Nutr* **17**, 141-158

11. van Tilbeurgh, H., Egloff, M. P., Martinez, C., Rugani, N., Verger, R., and Cambillau, C. (1993) Interfacial activation of the lipase-procolipase complex by mixed micelles revealed by X-ray crystallography. *Nature* **362**, 814-820

12. Bou Ali, M., Karray, A., Gargouri, Y., and Ben Ali, Y. (2013) N-terminal domain of turkey pancreatic lipase is active on long chain triacylglycerols and stabilized by colipase. *PloS one* **8**, e71605

13. Yang, Y., and Lowe, M. E. (2000) The open lid mediates pancreatic lipase function. *J Lipid Res* **41**, 48-57

14. Roy, A., Kucukural, A., and Zhang, Y. (2010) I-TASSER: a unified platform for automated protein structure and function prediction. *Nat Protoc* **5**, 725-738

15. Yang, J., Yan, R., Roy, A., Xu, D., Poisson, J., and Zhang, Y. (2015) The I-TASSER Suite: protein structure and function prediction. *Nat Methods* **12**, 7-8

16. Yang, J., and Zhang, Y. (2015) I-TASSER server: new development for protein structure and function predictions. *Nucleic Acids Res* **43**, W174-181

17. Zhang, Y. (2008) I-TASSER server for protein 3D structure prediction. *BMC Bioinformatics* **9**, 40

18. Voss, C. V., Davies, B. S., Tat, S., Gin, P., Fong, L. G., Pelletier, C., Mottler, C. D., Bensadoun, A., Beigneux, A. P., and Young, S. G. (2011) Mutations in lipoprotein lipase that block binding to the endothelial cell transporter GPIHBP1. *Proc Natl Acad Sci U S A* **108**, 7980-7984

19. Nielsen, M. S., Brejning, J., Garcia, R., Zhang, H., Hayden, M. R., Vilaro, S., and Gliemann, J. (1997) Segments in the C-terminal folding domain of lipoprotein lipase important for binding to the low density lipoprotein receptor-related protein and to heparan sulfate proteoglycans. *The Journal of biological chemistry* **272**, 5821-5827

20. Lookene, A., Groot, N. B., Kastelein, J. J., Olivecrona, G., and Bruin, T. (1997) Mutation of tryptophan residues in lipoprotein lipase. Effects on stability, immunoreactivity, and catalytic properties. *J Biol Chem* **272**, 766-772

21. Lookene, A., Zhang, L., Hultin, M., and Olivecrona, G. (2004) Rapid subunit exchange in dimeric lipoprotein lipase and properties of the inactive monomer. *J Biol Chem* **279**, 49964-49972

22. Griffon, N., Budreck, E. C., Long, C. J., Broedl, U. C., Marchadier, D. H., Glick, J. M., and Rader, D. J. (2006) Substrate specificity of lipoprotein lipase and endothelial lipase: studies of lid chimeras. *J Lipid Res* **47**, 1803-1811

23. Dugi, K. A., Dichek, H. L., and Santamarina-Fojo, S. (1995) Human hepatic and lipoprotein lipase: the loop covering the catalytic site mediates lipase substrate specificity. *J Biol Chem* **270**, 25396-25401

24. Kobayashi, Y., Nakajima, T., and Inoue, I. (2002) Molecular modeling of the dimeric structure of human lipoprotein lipase and functional studies of the carboxyl-terminal domain. *Eur J Biochem* **269**, 4701-4710

25. Dugi, K. A., Dichek, H. L., Talley, G. D., Brewer, H. B., Jr., and Santamarina-Fojo, S. (1992) Human lipoprotein lipase: the loop covering the catalytic site is essential for interaction with lipid substrates. *J Biol Chem* **267**, 25086-25091

26. Doolittle, M. H., Ehrhardt, N., and Peterfy, M. (2010) Lipase maturation factor 1: structure and role in lipase folding and assembly. *Curr Opin Lipidol* **21**, 198-203

27. Scow, R. O., Schultz, C. J., Park, J. W., and Blanchette-Mackie, E. J. (1998) Combined lipase deficiency (cld/cld) in mice affects differently post-translational processing of lipoprotein lipase, hepatic lipase and pancreatic lipase. *Chemistry and physics of lipids* **93**, 149-155

28. Picariello, G., Ferranti, P., Mamone, G., Roepstorff, P., and Addeo, F. (2008) Identification of N-linked glycoproteins in human milk by hydrophilic interaction liquid chromatography and mass spectrometry. *Proteomics* **8**, 3833-3847

29. Hubacek, J. A. (2016) Apolipoprotein A5 fifteen years anniversary: Lessons from genetic epidemiology. *Gene* **592**, 193-199

30. Nilsson, S. K., Heeren, J., Olivecrona, G., and Merkel, M. (2011) Apolipoprotein A-V; a potent triglyceride reducer. *Atherosclerosis* **219**, 15-21

31. Lookene, A., Beckstead, J. A., Nilsson, S., Olivecrona, G., and Ryan, R. O. (2005) Apolipoprotein A-V-heparin interactions: implications for plasma lipoprotein metabolism. *J Biol Chem* **280**, 25383-25387

32. O'Brien, P. J., Alborn, W. E., Sloan, J. H., Ulmer, M., Boodhoo, A., Knierman, M. D., Schultze, A. E., and Konrad, R. J. (2005) The novel apolipoprotein A5 is present in human serum, is associated with VLDL, HDL, and chylomicrons, and circulates at very low concentrations compared with other apolipoproteins. *Clinical chemistry* **51**, 351-359

33. Olivecrona, G., and Beisiegel, U. (1997) Lipid binding of apolipoprotein CII is required for stimulation of lipoprotein lipase activity against apolipoprotein CII-deficient chylomicrons. *Arteriosclerosis, thrombosis, and vascular biology* **17**, 1545-1549

34. McIlhargey, T. L., Yang, Y., Wong, H., and Hill, J. S. (2003) Identification of a lipoprotein lipase cofactor-binding site by chemical cross-linking and transfer of apolipoprotein C-II-responsive lipolysis from lipoprotein lipase to hepatic lipase. *J Biol Chem* **278**, 23027-23035

35. Shen, Y., Lookene, A., Nilsson, S., and Olivecrona, G. (2002) Functional analyses of human apolipoprotein CII by site-directed mutagenesis: identification of residues important for activation of lipoprotein lipase. *J Biol Chem* **277**, 4334-4342

36. Sakurai, T., Sakurai, A., Vaisman, B. L., Amar, M. J., Liu, C., Gordon, S. M., Drake, S. K., Pryor, M., Sampson, M. L., Yang, L., Freeman, L. A., and Remaley, A. T. (2016) Creation of Apolipoprotein C-II (ApoC-II) Mutant Mice and Correction of Their Hypertriglyceridemia with an ApoC-II Mimetic Peptide. *The Journal of Pharmacology and Experimental Therapeutics* **356**, 341-353

37. Kersten, S. (2014) Physiological regulation of lipoprotein lipase. *Biochim Biophys Acta* **1841**, 919-933

38. Wang, C. S., McConathy, W. J., Kloer, H. U., and Alaupovic, P. (1985) Modulation of lipoprotein lipase activity by apolipoproteins. Effect of apolipoprotein C-III. *The Journal of clinical investigation* **75**, 384-390

39. Jong, M. C., Hofker, M. H., and Havekes, L. M. (1999) Role of ApoCs in lipoprotein metabolism: functional differences between ApoC1, ApoC2, and ApoC3. *Arteriosclerosis, thrombosis, and vascular biology* **19**, 472-484

40. Berbée, J. F. P., van der Hoogt, C. C., Sundararaman, D., Havekes, L. M., and Rensen, P. C. N. (2005) Severe hypertriglyceridemia in human APOC1 transgenic mice is caused by apoC-I-induced inhibition of LPL. *Journal of Lipid Research* **46**, 297-306

41. Larsson, M., Vorrsjo, E., Talmud, P., Lookene, A., and Olivecrona, G. (2013) Apolipoproteins C-I and C-III inhibit lipoprotein lipase activity by displacement of the enzyme from lipid droplets. *J Biol Chem* **288**, 33997-34008

42. Dijk, W., and Kersten, S. (2016) Regulation of lipid metabolism by angiopoietin-like proteins. *Curr Opin Lipidol* **27**, 249-256

43. Westerterp, M., Berbee, J. F., Delsing, D. J., Jong, M. C., Gijbels, M. J., Dahlmans, V. E., Offerman, E. H., Romijn, J. A., Havekes, L. M., and Rensen, P. C. (2007) Apolipoprotein C-I binds free fatty acids and reduces their intracellular esterification. *J Lipid Res* **48**, 1353-1361

44. van Ree, J. H., Hofker, M. H., van den Broek, W. J., van Deursen, J. M., van der Boom, H., Frants, R. R., Wieringa, B., and Havekes, L. M. (1995) Increased response to cholesterol feeding in apolipoprotein C1-deficient mice. *The Biochemical journal* **305 (Pt 3)**, 905-911

45. Yang, X., Lee, S. R., Choi, Y. S., Alexander, V. J., Digenio, A., Yang, Q., Miller, Y. I., Witztum, J. L., and Tsimikas, S. (2016) Reduction in lipoprotein-associated apoC-III levels following volanesorsen therapy: phase 2 randomized trial results. *J Lipid Res* **57**, 706-713

46. Schmitz, J., and Gouni-Berthold, I. (2017) Apoc-III antisense oligonucleotides: a new option for the treatment of hypertriglyceridemia. *Current medicinal chemistry*

47. Koster, A., Chao, Y. B., Mosior, M., Ford, A., Gonzalez-DeWhitt, P. A., Hale, J. E., Li, D., Qiu, Y., Fraser, C. C., Yang, D. D., Heuer, J. G., Jaskunas, S. R., and Eacho, P. (2005) Transgenic angiopoietin-like (angptl)4 overexpression and targeted disruption of angptl4 and angptl3: regulation of triglyceride metabolism. *Endocrinology* **146**, 4943-4950

48. Fujimoto, K., Koishi, R., Shimizugawa, T., and Ando, Y. (2006) Angptl3-null mice show low plasma lipid concentrations by enhanced lipoprotein lipase activity. *Experimental animals* **55**, 27-34

49. Haller, J. F., Mintah, I. J., Shihanian, L. M., Stevis, P., Buckler, D., Alexa-Braun, C. A., Kleiner, S., Banfi, S., Cohen, J. C., Hobbs, H. H., Yancopoulos, G. D., Murphy, A. J., Gusarova, V., and Gromada, J. (2017) ANGPTL8 requires ANGPTL3 to inhibit lipoprotein lipase and plasma triglyceride clearance. *J Lipid Res* **58**, 1166-1173

50. Quagliarini, F., Wang, Y., Kozlitina, J., Grishin, N. V., Hyde, R., Boerwinkle, E., Valenzuela, D. M., Murphy, A. J., Cohen, J. C., and Hobbs, H. H. (2012)

Atypical angiopoietin-like protein that regulates ANGPTL3. *Proc Natl Acad Sci U S A* **109**, 19751-19756

51. Zhang, R. (2016) The ANGPTL3-4-8 model, a molecular mechanism for triglyceride trafficking. *Open biology* **6**, 150272

52. Fu, Z., Abou-Samra, A. B., and Zhang, R. (2015) A lipasin/Angptl8 monoclonal antibody lowers mouse serum triglycerides involving increased postprandial activity of the cardiac lipoprotein lipase. *Scientific reports* **5**, 18502

53. Lafferty, M. J., Bradford, K. C., Erie, D. A., and Neher, S. B. (2013) Angiopoietin-like protein 4 inhibition of lipoprotein lipase: evidence for reversible complex formation. *J Biol Chem* **288**, 28524-28534

54. Mattijssen, F., Alex, S., Swarts, H. J., Groen, A. K., van Schothorst, E. M., and Kersten, S. (2014) Angptl4 serves as an endogenous inhibitor of intestinal lipid digestion. *Molecular metabolism* **3**, 135-144

55. Stitziel, N. O., Stirrups, K. E., Masca, N. G., Erdmann, J., Ferrario, P. G., Konig, I. R., Weeke, P. E., Webb, T. R., Auer, P. L., Schick, U. M., Lu, Y., Zhang, H., Dube, M. P., Goel, A., Farrall, M., Peloso, G. M., Won, H. H., Do, R., van Iperen, E., Kanoni, S., Kruppa, J., Mahajan, A., Scott, R. A., Willenberg, C., Braund, P. S., van Capelleveen, J. C., Doney, A. S., Donnelly, L. A., Asselta, R., Merlini, P. A., Duga, S., Marziliano, N., Denny, J. C., Shaffer, C. M., El-Mokhtari, N. E., Franke, A., Gottesman, O., Heilmann, S., Hengstenberg, C., Hoffman, P., Holmen, O. L., Hveem, K., Jansson, J. H., Jockel, K. H., Kessler, T., Kriebel, J., Laugwitz, K. L., Marouli, E., Martinelli, N., McCarthy, M. I., Van Zuydam, N. R., Meisinger, C., Esko, T., Mihailov, E., Escher, S. A., Alver, M., Moebus, S., Morris, A. D., Muller-Nurasyid, M., Nikpay, M., Olivieri, O., Lemieux Perreault, L. P., AlQarawi, A., Robertson, N. R., Akinsanya, K. O., Reilly, D. F., Vogt, T. F., Yin, W., Asselbergs, F. W., Kooperberg, C., Jackson, R. D., Stahl, E., Strauch, K., Varga, T. V., Waldenberger, M., Zeng, L., Kraja, A. T., Liu, C., Ehret, G. B., Newton-Cheh, C., Chasman, D. I., Chowdhury, R., Ferrario, M., Ford, I., Jukema, J. W., Kee, F., Kuulasmaa, K., Nordestgaard, B. G., Perola, M., Saleheen, D., Sattar, N., Surendran, P., Tregouet, D., Young, R., Howson, J. M., Butterworth, A. S., Danesh, J., Ardissino, D., Bottinger, E. P., Erbel, R., Franks, P. W., Girelli, D., Hall, A. S., Hovingh, G. K., Kastrati, A., Lieb, W., Meitinger, T., Kraus, W. E., Shah, S. H., McPherson, R., Orho-Melander, M., Melander, O., Metspalu, A., Palmer, C. N., Peters, A., Rader, D., Reilly, M. P., Loos, R. J., Reiner, A. P., Roden, D. M., Tardif, J. C., Thompson, J. R., Wareham, N. J., Watkins, H., Willer, C. J., Kathiresan, S., Deloukas, P., Samani, N. J., and Schunkert, H. (2016) Coding Variation in ANGPTL4, LPL, and SVEP1 and the Risk of Coronary Disease. *The New England journal of medicine* **374**, 1134-1144

56.   Nilsson, S. K., Anderson, F., Ericsson, M., Larsson, M., Makoveichuk, E., Lookene, A., Heeren, J., and Olivecrona, G. (2012) Triacylglycerol-rich lipoproteins protect lipoprotein lipase from inactivation by ANGPTL3 and ANGPTL4. *Biochim Biophys Acta* **1821**, 1370-1378

57.   Sonnenburg, W. K., Yu, D., Lee, E. C., Xiong, W., Gololobov, G., Key, B., Gay, J., Wilganowski, N., Hu, Y., Zhao, S., Schneider, M., Ding, Z. M., Zambrowicz, B. P., Landes, G., Powell, D. R., and Desai, U. (2009) GPIHBP1 stabilizes lipoprotein lipase and prevents its inhibition by angiopoietin-like 3 and angiopoietin-like 4. *J Lipid Res* **50**, 2421-2429

58.   Chi, X., Shetty, S. K., Shows, H. W., Hjelmaas, A. J., Malcolm, E. K., and Davies, B. S. (2015) Angiopoietin-like 4 Modifies the Interactions between Lipoprotein Lipase and Its Endothelial Cell Transporter GPIHBP1. *J Biol Chem* **290**, 11865-11877

59.   Burnett, J. R., and Hooper, A. J. (2009) Alipogene tiparvovec, an adeno-associated virus encoding the Ser(447)X variant of the human lipoprotein lipase gene for the treatment of patients with lipoprotein lipase deficiency. *Curr Opin Mol Ther* **11**, 681-691

60.   Hayne, C. K., Lafferty, M. J., Eglinger, B. J., Kane, J. P., and Neher, S. B. (2017) Biochemical Analysis of the Lipoprotein Lipase Truncation Variant, LPLS447X, Reveals Increased Lipoprotein Uptake. *Biochemistry* **56**, 525-533

61.   Gaudet, D., Methot, J., Dery, S., Brisson, D., Essiembre, C., Tremblay, G., Tremblay, K., de Wal, J., Twisk, J., van den Bulk, N., Sier-Ferreira, V., and van Deventer, S. (2013) Efficacy and long-term safety of alipogene tiparvovec (AAV1-LPLS447X) gene therapy for lipoprotein lipase deficiency: an open-label trial. *Gene Ther* **20**, 361-369

62.   Ferreira, V., Twisk, J., Kwikkers, K., Aronica, E., Brisson, D., Methot, J., Petry, H., and Gaudet, D. (2014) Immune responses to intramuscular administration of alipogene tiparvovec (AAV1-LPL(S447X)) in a phase II clinical trial of lipoprotein lipase deficiency gene therapy. *Hum Gene Ther* **25**, 180-188

63.   Gaudet, D., Stroes, E. S., Methot, J., Brisson, D., Tremblay, K., Bernelot Moens, S. J., Iotti, G., Rastelletti, I., Ardigo, D., Corzo, D., Meyer, C., Andersen, M., Ruszniewski, P., Deakin, M., and Bruno, M. J. (2016) Long-Term Retrospective Analysis of Gene Therapy with Alipogene Tiparvovec and Its Effect on Lipoprotein Lipase Deficiency-Induced Pancreatitis. *Hum Gene Ther* **27**, 916-925

64.   Nocon-Bohusz, J., Wikiera, B., Basiak, A., Smigiel, R., and Noczynska, A. (2016) LPL gene mutation as the cause of severe hypertriglyceridemia in the

course of ketoacidosis in a patient with newly diagnosed type 1 diabetes mellitus. *Pediatr Endocrinol Diabetes Metab* **21**, 89-92

65.   Larsson, M., Caraballo, R., Ericsson, M., Lookene, A., Enquist, P.-A., Elofsson, M., Nilsson, S. K., and Olivecrona, G. (2014) Identification of a small molecule that stabilizes lipoprotein lipase in vitro and lowers triglycerides in vivo. *Biochemical and Biophysical Research Communications* **450**, 1063-1069

66.   Graham, M. J., Lee, R. G., Bell, T. A., 3rd, Fu, W., Mullick, A. E., Alexander, V. J., Singleton, W., Viney, N., Geary, R., Su, J., Baker, B. F., Burkey, J., Crooke, S. T., and Crooke, R. M. (2013) Antisense oligonucleotide inhibition of apolipoprotein C-III reduces plasma triglycerides in rodents, nonhuman primates, and humans. *Circ Res* **112**, 1479-1490

67.   Amar, M. J., Sakurai, T., Sakurai-Ikuta, A., Sviridov, D., Freeman, L., Ahsan, L., and Remaley, A. T. (2015) A novel apolipoprotein C-II mimetic peptide that activates lipoprotein lipase and decreases serum triglycerides in apolipoprotein E-knockout mice. *The Journal of Pharmacology and Experimental Therapeutics* **352**, 227-235

68.   Caraballo, R., Larsson, M., Nilsson, S. K., Ericsson, M., Qian, W., Nguyen Tran, N. P., Kindahl, T., Svensson, R., Saar, V., Artursson, P., Olivecrona, G., Enquist, P. A., and Elofsson, M. (2015) Structure-activity relationships for lipoprotein lipase agonists that lower plasma triglycerides in vivo. *Eur J Med Chem* **103**, 191-209

69.   Carroll MD, K. B., Lacher DA. . (2015) Trends in Elevated Triglyceride in Adults: United States, 2001–2012. *NCHS data brief* **198**

70.   Kozaki, K., Gotoda, T., Kawamura, M., Shimano, H., Yazaki, Y., Ouchi, Y., Orimo, H., and Yamada, N. (1993) Mutational analysis of human lipoprotein lipase by carboxy-terminal truncation. *J Lipid Res* **34**, 1765-1772

71.   Rip, J., Nierman, M. C., Ross, C. J., Jukema, J. W., Hayden, M. R., Kastelein, J. J., Stroes, E. S., and Kuivenhoven, J. A. (2006) Lipoprotein lipase S447X: a naturally occurring gain-of-function mutation. *Arteriosclerosis, thrombosis, and vascular biology* **26**, 1236-1245

72.   Gagne, S. E., Larson, M. G., Pimstone, S. N., Schaefer, E. J., Kastelein, J. J., Wilson, P. W., Ordovas, J. M., and Hayden, M. R. (1999) A common truncation variant of lipoprotein lipase (Ser447X) confers protection against coronary heart disease: the Framingham Offspring Study. *Clin Genet* **55**, 450-454

73. Yang, Y., Ruiz-Narvaez, E., Niu, T., Xu, X., and Campos, H. (2004) Genetic variants of the lipoprotein lipase gene and myocardial infarction in the Central Valley of Costa Rica. *J Lipid Res* **45**, 2106-2109

74. Ross, C. J., Liu, G., Kuivenhoven, J. A., Twisk, J., Rip, J., van Dop, W., Excoffon, K. J., Lewis, S. M., Kastelein, J. J., and Hayden, M. R. (2005) Complete rescue of lipoprotein lipase-deficient mice by somatic gene transfer of the naturally occurring LPLS447X beneficial mutation. *Arteriosclerosis, thrombosis, and vascular biology* **25**, 2143-2150

75. Ranganathan, G., Unal, R., Pokrovskaya, I. D., Tripathi, P., Rotter, J. I., Goodarzi, M. O., and Kern, P. A. (2012) The lipoprotein lipase (LPL) S447X gain of function variant involves increased mRNA translation. *Atherosclerosis* **221**, 143-147

76. Previato, L., Guardamagna, O., Dugi, K. A., Ronan, R., Talley, G. D., Santamarina-Fojo, S., and Brewer, H. B., Jr. (1994) A novel missense mutation in the C-terminal domain of lipoprotein lipase (Glu410-->Val) leads to enzyme inactivation and familial chylomicronemia. *J Lipid Res* **35**, 1552-1560

77. Zhang, H., Henderson, H., Gagne, S. E., Clee, S. M., Miao, L., Liu, G., and Hayden, M. R. (1996) Common sequence variants of lipoprotein lipase: standardized studies of in vitro expression and catalytic function. *Biochimica et Biophysica Acta (BBA) - Lipids and Lipid Metabolism* **1302**, 159-166

78. Kobayashi, J., Nishida, T., Ameis, D., Stahnke, G., Schotz, M. C., Hashimoto, H., Fukamachi, I., Shirai, K., Saito, Y., and Yoshida, S. (1992) A heterozygous mutation (the codon for Ser447----a stop codon) in lipoprotein lipase contributes to a defect in lipid interface recognition in a case with type I hyperlipidemia. *Biochem Biophys Res Commun* **182**, 70-77

79. Turlo, K., Leung, C. S., Seo, J. J., Goulbourne, C. N., Adeyo, O., Gin, P., Voss, C., Bensadoun, A., Fong, L. G., Young, S. G., and Beigneux, A. P. (2014) Equivalent binding of wild-type lipoprotein lipase (LPL) and S447X-LPL to GPIHBP1, the endothelial cell LPL transporter. *Biochim Biophys Acta* **1841**, 963-969

80. Faustinella, F., Chang, A., Van Biervliet, J. P., Rosseneu, M., Vinaimont, N., Smith, L. C., Chen, S. H., and Chan, L. (1991) Catalytic triad residue mutation (Asp156----Gly) causing familial lipoprotein lipase deficiency. Co-inheritance with a nonsense mutation (Ser447----Ter) in a Turkish family. *J Biol Chem* **266**, 14418-14424

81.   Jin, W., Fuki, I. V., Seidah, N. G., Benjannet, S., Glick, J. M., and Rader, D. J. (2005) Proprotein convertases [corrected] are responsible for proteolysis and inactivation of endothelial lipase. *J Biol Chem* **280**, 36551-36559

82.   Chappell, D. A., Fry, G. L., Waknitz, M. A., Muhonen, L. E., Pladet, M. W., Iverius, P. H., and Strickland, D. K. (1993) Lipoprotein lipase induces catabolism of normal triglyceride-rich lipoproteins via the low density lipoprotein receptor-related protein/alpha 2-macroglobulin receptor in vitro. A process facilitated by cell-surface proteoglycans. *The Journal of biological chemistry* **268**, 14168-14175

83.   Beisiegel, U., Weber, W., Ihrke, G., Herz, J., and Stanley, K. K. (1989) The LDL-receptor-related protein, LRP, is an apolipoprotein E-binding protein. *Nature* **341**, 162-164

84.   Nierman, M. C., Prinsen, B. H., Rip, J., Veldman, R. J., Kuivenhoven, J. A., Kastelein, J. J., de Sain-van der Velden, M. G., and Stroes, E. S. (2005) Enhanced conversion of triglyceride-rich lipoproteins and increased low-density lipoprotein removal in LPLS447X carriers. *Arteriosclerosis, thrombosis, and vascular biology* **25**, 2410-2415

85.   Bengtsson-Olivecrona, G., and Olivecrona, T. (1991) Phospholipase activity of milk lipoprotein lipase. *Methods Enzymol* **197**, 345-356

86.   Bensadoun, A., Mottler, C. D., Pelletier, C., Wu, D., Seo, J. J., Leung, C. S., Adeyo, O., Goulbourne, C. N., Gin, P., Fong, L. G., Young, S. G., and Beigneux, A. P. (2014) A new monoclonal antibody, 4-1a, that binds to the amino terminus of human lipoprotein lipase. *Biochim Biophys Acta* **1841**, 970-976

87.   Chung, B. H., Wilkinson, T., Geer, J. C., and Segrest, J. P. (1980) Preparative and quantitative isolation of plasma lipoproteins: rapid, single discontinuous density gradient ultracentrifugation in a vertical rotor. *J Lipid Res* **21**, 284-291

88.   Garrett, C. K., Broadwell, L. J., Hayne, C. K., and Neher, S. B. (2015) Modulation of the Activity of Mycobacterium tuberculosis LipY by Its PE Domain. *PloS one* **10**, e0135447

89.   Johnson, J. D., Taskinen, M. R., Matsuoka, N., and Jackson, R. L. (1980) Dansyl phosphatidylethanolamine-labeled very low density lipoproteins. A fluorescent probe for monitoring lipolysis. *J Biol Chem* **255**, 3461-3465

90.   Kleiger, G., Saha, A., Lewis, S., Kuhlman, B., and Deshaies, R. J. (2009) Rapid E2-E3 assembly and disassembly enable processive ubiquitylation of cullin-RING ubiquitin ligase substrates. *Cell* **139**, 957-968

91.   Kidd, D., Liu, Y., and Cravatt, B. F. (2001) Profiling serine hydrolase activities in complex proteomes. *Biochemistry* **40**, 4005-4015

92.   Loeffler, B., Heeren, J., Blaeser, M., Radner, H., Kayser, D., Aydin, B., and Merkel, M. (2007) Lipoprotein lipase-facilitated uptake of LDL is mediated by the LDL receptor. *J Lipid Res* **48**, 288-298

93.   Lookene, A., Nielsen, M. S., Gliemann, J., and Olivecrona, G. (2000) Contribution of the carboxy-terminal domain of lipoprotein lipase to interaction with heparin and lipoproteins. *Biochem Biophys Res Commun* **271**, 15-21

94.   Wittrup, H. H., Nordestgaard, B. G., Steffensen, R., Jensen, G., and Tybjaerg-Hansen, A. (2002) Effect of gender on phenotypic expression of the S447X mutation in LPL: the Copenhagen City Heart Study. *Atherosclerosis* **165**, 119-126

95.   Stroes, E. S., Nierman, M. C., Meulenberg, J. J., Franssen, R., Twisk, J., Henny, C. P., Maas, M. M., Zwinderman, A. H., Ross, C., Aronica, E., High, K. A., Levi, M. M., Hayden, M. R., Kastelein, J. J., and Kuivenhoven, J. A. (2008) Intramuscular administration of AAV1-lipoprotein lipase S447X lowers triglycerides in lipoprotein lipase-deficient patients. *Arteriosclerosis, thrombosis, and vascular biology* **28**, 2303-2304

96.   Nierman, M. C., Rip, J., Kuivenhoven, J. A., van Raalte, D. H., Hutten, B. A., Sakai, N., Kastelein, J. J., and Stroes, E. S. (2005) Carriers of the frequent lipoprotein lipase S447X variant exhibit enhanced postprandial apoprotein B-48 clearance. *Metabolism* **54**, 1499-1503

97.   Takahashi, S., Suzuki, J., Kohno, M., Oida, K., Tamai, T., Miyabo, S., Yamamoto, T., and Nakai, T. (1995) Enhancement of the binding of triglyceride-rich lipoproteins to the very low density lipoprotein receptor by apolipoprotein E and lipoprotein lipase. *The Journal of biological chemistry* **270**, 15747-15754

98.   Chappell, D. A., Inoue, I., Fry, G. L., Pladet, M. W., Bowen, S. L., Iverius, P. H., Lalouel, J. M., and Strickland, D. K. (1994) Cellular catabolism of normal very low density lipoproteins via the low density lipoprotein receptor-related protein/alpha 2-macroglobulin receptor is induced by the C-terminal domain of lipoprotein lipase. *J Biol Chem* **269**, 18001-18006

99.   Boren, J., Lookene, A., Makoveichuk, E., Xiang, S., Gustafsson, M., Liu, H., Talmud, P., and Olivecrona, G. (2001) Binding of low density lipoproteins to lipoprotein lipase is dependent on lipids but not on apolipoprotein B. *J Biol Chem* **276**, 26916-26922

100. Reimund, M., Larsson, M., Kovrov, O., Kasvandik, S., Olivecrona, G., and Lookene, A. (2015) Evidence for Two Distinct Binding Sites for Lipoprotein Lipase on Glycosylphosphatidylinositol-anchored High Density Lipoprotein-binding Protein 1 (GPIHBP1). *J Biol Chem* **290**, 13919-13934

101. Roy, R., Hohng, S., and Ha, T. (2008) A practical guide to single-molecule FRET. *Nat Meth* **5**, 507-516

102. DeRocco, V., Anderson, T., Piehler, J., Erie, D. A., and Weninger, K. (2010) Four-color single-molecule fluorescence with noncovalent dye labeling to monitor dynamic multimolecular complexes. *Biotechniques* **49**, 807-816

103. Sass, L. E., Lanyi, C., Weninger, K., and Erie, D. A. (2010) Single-molecule FRET TACKLE reveals highly dynamic mismatched DNA-MutS complexes. *Biochemistry* **49**, 3174-3190

104. Ha, T., Kozlov, A. G., and Lohman, T. M. (2012) Single-molecule views of protein movement on single-stranded DNA. *Annu Rev Biophys* **41**, 295-319

105. Erie, D. A., and Weninger, K. R. (2014) Single molecule studies of DNA mismatch repair. *DNA Repair (Amst)* **20**, 71-81

106. Liao, J. Y., Song, Y., and Liu, Y. (2015) A new trend to determine biochemical parameters by quantitative FRET assays. *Acta Pharmacol Sin* **36**, 1408-1415

107. Piraino, M. S., Kelliher, M. T., Aburas, J., and Southern, C. A. (2015) Single molecule Forster resonance energy transfer studies of the effect of EndoS deglycosylation on the structure of IgG. *Immunol Lett* **167**, 29-33

108. Sadler, E. E., Kapanidis, A. N., and Tucker, S. J. (2016) Solution-Based Single-Molecule FRET Studies of K(+) Channel Gating in a Lipid Bilayer. *Biophys J* **110**, 2663-2670

109. Lehninger, A., Nelson, D., and Cox, M. (2008) *Lehninger Principles of Biochemistry*, W. H. Freeman

110. Choi, U. B., Strop, P., Vrljic, M., Chu, S., Brunger, A. T., and Weninger, K. R. (2010) Single-molecule FRET-derived model of the synaptotagmin 1-SNARE fusion complex. *Nat Struct Mol Biol* **17**, 318-324

111. Brunger, A. T., Strop, P., Vrljic, M., Chu, S., and Weninger, K. R. (2011) Three-dimensional molecular modeling with single molecule FRET. *J Struct Biol* **173**, 497-505

112. Ross, J., Buschkamp, P., Fetting, D., Donnermeyer, A., Roth, C. M., and Tinnefeld, P. (2007) Multicolor Single-Molecule Spectroscopy with Alternating

Laser Excitation for the Investigation of Interactions and Dynamics. *The Journal of Physical Chemistry B* **111**, 321-326

113. Friedman, L. J., Chung, J., and Gelles, J. (2006) Viewing dynamic assembly of molecular complexes by multi-wavelength single-molecule fluorescence. *Biophys J* **91**, 1023-1031

114. Friedman, L. J., and Gelles, J. (2012) Mechanism of transcription initiation at an activator-dependent promoter defined by single-molecule observation. *Cell* **148**, 679-689

115. Tinoco, I., Jr., and Gonzalez, R. L., Jr. (2011) Biological mechanisms, one molecule at a time. *Genes Dev* **25**, 1205-1231

116. Joo, C., Balci, H., Ishitsuka, Y., Buranachai, C., and Ha, T. (2008) Advances in single-molecule fluorescence methods for molecular biology. *Annu Rev Biochem* **77**, 51-76

117. Joo, C., and Ha, T. (2012) Single-molecule FRET with total internal reflection microscopy. *Cold Spring Harb Protoc* **2012**

118. Kim, H., and Ha, T. (2013) Single molecule nanometry for biological physics. *Rep Prog Phys* **76**, 016601

119. Weninger, K., Bowen, M. E., Chu, S., and Brunger, A. T. (2003) Single-molecule studies of SNARE complex assembly reveal parallel and antiparallel configurations. *Proc Natl Acad Sci U S A* **100**, 14800-14805

120. Hayne, C. K., Lafferty, M. J., Eglinger, B. J., Kane, J. P., and Neher, S. B. (2017) Biochemical Analysis of the Lipoprotein Lipase Truncation Variant, LPLS447X, Reveals Increased Lipoprotein Uptake. *Biochemistry*

121. Bowen, M. E., Weninger, K., Ernst, J., Chu, S., and Brunger, A. T. (2005) Single-molecule studies of synaptotagmin and complexin binding to the SNARE complex. *Biophys J* **89**, 690-702

122. Chung, S. H., and Kennedy, R. A. (1991) Forward-backward non-linear filtering technique for extracting small biological signals from noise. *J Neurosci Methods* **40**, 71-86

123. Haran, G. (2004) Noise reduction in single-molecule fluorescence trajectories of folding proteins. *Chemical Physics* **307**, 137-145

124. Bengtsson-Olivecrona, G., and Olivecrona, T. (1985) Binding of active and inactive forms of lipoprotein lipase to heparin. Effects of pH. *The Biochemical journal* **226**, 409-413

125. Shcherbakova, I., Hoskins, A. A., Friedman, L. J., Serebrov, V., Correa, I. R., Jr., Xu, M. Q., Gelles, J., and Moore, M. J. (2013) Alternative spliceosome assembly pathways revealed by single-molecule fluorescence microscopy. *Cell Rep* **5**, 151-165

126. Xie, S. (2001) Single-Molecule Approach to Enzymology. *Single Molecules* **2**, 229-236

127. Stein, I. H., Steinhauer, C., and Tinnefeld, P. (2011) Single-Molecule Four-Color FRET Visualizes Energy-Transfer Paths on DNA Origami. *Journal of the American Chemical Society* **133**, 4193-4195

128. Hohng, S., Joo, C., and Ha, T. (2004) Single-molecule three-color FRET. *Biophys J* **87**, 1328-1337

129. Ratzke, C., Hellenkamp, B., and Hugel, T. (2014) Four-colour FRET reveals directionality in the Hsp90 multicomponent machinery. *Nat Commun* **5**

130. Floyd, D. L., Harrison, S. C., and van Oijen, A. M. (2010) Analysis of kinetic intermediates in single-particle dwell-time distributions. *Biophys J* **99**, 360-366

131. van Tilbeurgh, H., Roussel, A., Lalouel, J. M., and Cambillau, C. (1994) Lipoprotein lipase. Molecular model based on the pancreatic lipase x-ray structure: consequences for heparin binding and catalysis. *J Biol Chem* **269**, 4626-4633

132. van Zundert, G. C. P., Rodrigues, J. P. G. L. M., Trellet, M., Schmitz, C., Kastritis, P. L., Karaca, E., Melquiond, A. S. J., van Dijk, M., de Vries, S. J., and Bonvin, A. M. J. J. (2016) The HADDOCK2.2 Web Server: User-Friendly Integrative Modeling of Biomolecular Complexes. *Journal of Molecular Biology* **428**, 720-725

133. Lutz, E. P., Kako, Y., Yagyu, H., Heeren, J., Marks, S., Wright, T., Melford, K., Ben-Zeev, O., Radner, H., Merkel, M., Bensadoun, A., Wong, H., and Goldberg, I. J. (2004) Mice expressing only covalent dimeric heparin binding-deficient lipoprotein lipase: muscles inefficiently secrete dimeric enzyme. *J Biol Chem* **279**, 238-244

134. Basu, D., Manjur, J., and Jin, W. (2011) Determination of lipoprotein lipase activity using a novel fluorescent lipase assay. *J Lipid Res* **52**, 826-832

135. Nierman, M. C., Rip, J., Kuivenhoven, J. A., Sakai, N., Kastelein, J. J., de Sain-van der Velden, M. G., Stroes, E. S., and Prinsen, B. H. (2007) Enhanced apoB48 metabolism in lipoprotein lipase X447 homozygotes. *Atherosclerosis* **194**, 446-451

136. Cohen, J. C., Boerwinkle, E., Mosley, T. H., Jr., and Hobbs, H. H. (2006) Sequence variations in PCSK9, low LDL, and protection against coronary heart disease. *The New England journal of medicine* **354**, 1264-1272

137. Cohen, J., Pertsemlidis, A., Kotowski, I. K., Graham, R., Garcia, C. K., and Hobbs, H. H. (2005) Low LDL cholesterol in individuals of African descent resulting from frequent nonsense mutations in PCSK9. *Nature genetics* **37**, 161-165

138. Jaworski, K., Jankowski, P., and Kosior, D. A. (2017) PCSK9 inhibitors - from discovery of a single mutation to a groundbreaking therapy of lipid disorders in one decade. *Archives of medical science : AMS* **13**, 914-929

139. Choi, J., Khan, A. M., Jarmin, M., Goldenberg, N., Glueck, C. J., and Wang, P. (2017) Efficacy and safety of proprotein convertase subtilisin-kexin type 9 (PCSK9) inhibitors, alirocumab and evolocumab, a post-commercialization study. *Lipids in health and disease* **16**, 141

140. Descamps, O. S., Fraass, U., Dent, R., Marz, W., and Gouni-Berthold, I. (2017) Anti-PCSK9 antibodies for hypercholesterolaemia: Overview of clinical data and implications for primary care. *International journal of clinical practice*

141. Chackerian, B., and Remaley, A. (2016) Vaccine strategies for lowering LDL by immunization against proprotein convertase subtilisin/kexin type 9. *Curr Opin Lipidol* **27**, 345-350

142. Crossey, E., Amar, M. J., Sampson, M., Peabody, J., Schiller, J. T., Chackerian, B., and Remaley, A. T. (2015) A cholesterol-lowering VLP vaccine that targets PCSK9. *Vaccine* **33**, 5747-5755

143. Chadwick, A. C., Wang, X., and Musunuru, K. (2017) In Vivo Base Editing of PCSK9 (Proprotein Convertase Subtilisin/Kexin Type 9) as a Therapeutic Alternative to Genome Editing. *Arteriosclerosis, thrombosis, and vascular biology*

144. Starr, A. E., Lemieux, V., Noad, J., Moore, J. I., Dewpura, T., Raymond, A., Chretien, M., Figeys, D., and Mayne, J. (2015) beta-Estradiol results in a proprotein convertase subtilisin/kexin type 9-dependent increase in low-density lipoprotein receptor levels in human hepatic HuH7 cells. *The FEBS journal* **282**, 2682-2696